J. metamorphic Geol., 2001, **19,** 233–248

Formation and exhumation of blueschists and eclogites from NE Oman: new perspectives from Rb–Sr and $^{40}Ar/^{39}Ar$ dating

A. K. EL-SHAZLY,[1]* M. BRÖCKER,[2] B. HACKER[3] AND A. CALVERT[3]
[1]*Department of Earth Sciences, Sultan Qaboos University, Oman, and Geology Department, Idaho State University, USA (aelshazly@utm.edu)*
[2]*Universität Münster, Institut für Mineralogie, D-48149 Münster, Germany*
[3]*Geological Sciences Department, University of California, Santa Barbara, CA 93106-9630, USA*

ABSTRACT Seven eclogite facies samples from lithologically different units which structurally underlie the Semail ophiolite were dated by the $^{40}Ar/^{39}Ar$ and Rb–Sr methods. Despite extensive efforts, phengite dated by the $^{40}Ar/^{39}Ar$ method yielded saddle, hump or irregularly shaped spectra with uninterpretable isochrons. The total gas ages for the phengite ranged from 136 to 85 Ma. Clinopyroxene–phengite, epidote–phengite and whole-rock–phengite Rb–Sr isochrons for the same samples yielded ages of 78 ± 2 Ma. We therefore conclude that the eclogite facies rocks cooled through 500 °C at *c.* 78 ± 2 Ma, and that the $^{40}Ar/^{39}Ar$ dates can only constrain maximum ages due to the occurrence of excess Ar inhomogeneously distributed in different sites. Our new results lead us to conclude that high-pressure metamorphism of the Oman margin took place in the Late Cretaceous, contemporaneous with ophiolite emplacement. Previously published structural and petrological data lead us to suggest that this metamorphism resulted from intracontinental subduction and crustal thickening along a NE-dipping zone. Choking of this subduction zone followed by ductile thinning of a crustal mass wedged between deeply subducted continental material and overthrust shelf and slope units facilitated the exhumation of the eclogite facies rocks from depths of *c.* 50 km to 10–15 km within *c.* 10 Ma, and led to their juxtaposition against overlying lower grade rocks. Final exhumation of all high-pressure rocks was driven primarily by erosion and assisted by normal faulting in the upper plate.

Key words: age data; blueschists; eclogites; exhumation; Oman; subduction.

INTRODUCTION

Since Michard *et al.* (1983) and Lippard (1983) reported the occurrence of Fe–Mg carpholite-bearing metasediments and blueschists in the Saih Hatat area in NE Oman, at least 10 different tectonic models have been proposed to explain the formation and exhumation of these high-pressure, low-temperature (high-P/T) metamorphic rocks. Although these models agree that the continental margin in NE Oman was subducted sometime in the Cretaceous, they disagree on such issues as subduction polarity and depth, and the timing of high-P/T metamorphism in relation to the emplacement of the Semail ophiolite (cf. Lippard *et al.*, 1986; Le Métour *et al.*, 1990; El-Shazly & Lanphere, 1992; Gregory *et al.*, 1998; Searle & Cox, 1999). The exhumation mechanism of these high-P/T rocks is also controversial (e.g. El-Shazly & Lanphere, 1992; Michard *et al.*, 1994; Chemenda *et al.*, 1996; Miller *et al.*, 1999).

One of the main reasons for the continued controversy over the tectonic history of NE Oman is that the age of peak metamorphism and the cooling rates of the high-P/T rocks are poorly constrained. High-P/T metamorphic rocks from Saih Hatat have so far been dated by K–Ar or $^{40}Ar/^{39}Ar$ methods on phengite separates, which yielded ages ranging from 131 to 72 Ma (Lippard, 1983; Montigny *et al.*, 1988; El-Shazly & Lanphere, 1992; Searle *et al.*, 1994; Miller *et al.*, 1999). El-Shazly & Lanphere (1992) interpreted ages as indicating two discrete high-P/T metamorphic events: an Early Cretaceous event resulting from the subduction of the north-eastern part of the Oman continental margin, and a weaker Late Cretaceous event related to ophiolite emplacement. Gregory *et al.* (1998) had similar interpretations for the older ages (131–82 Ma), but suggested that the continental margin was subducted in a SW-dipping zone before ophiolite emplacement. On the other hand, Goffé *et al.* (1988), Le Métour *et al.* (1990), Michard *et al.* (1994) and Searle *et al.* (1994) argued that phengite from the Oman blueschists and eclogites incorporated excess Ar, and attributed high-P/T metamorphism to Late Cretaceous subduction of the continental margin of Oman, either shortly before, or contemporaneous with, the emplacement of the ophiolite.

Most of the $^{40}Ar/^{39}Ar$ white mica spectra reported by Montigny *et al.* (1988) and El-Shazly & Lanphere (1992) are hump-shaped and do not always satisfy the criteria of Dalrymple & Lanphere (1974) for a meaningful age.

*Present address: Dept. of Geology, Geography & Physics, Univ. Tennessee, TN 38238.

Because other studies of high-pressure rocks have shown that incomplete degassing of mica grains, or the incorporation of excess ^{40}Ar, can produce similar hump-shaped spectra (e.g. Hacker & Wang, 1995; Hannula & McWilliams, 1995; Ruffet *et al.*, 1995), the $^{40}Ar/^{39}Ar$ ages of Montigny *et al.* (1988) and El-Shazly & Lanphere (1992) may not represent an actual geological event. The internal discordance of the Montigny *et al.* (1988) $^{40}Ar/^{39}Ar$ spectra indicates that their K/Ar ages, as well as those of Lippard (1983), cannot be relied upon to indicate the time of the high-pressure metamorphism. Although the white mica 96 ± 2 Ma age of Searle *et al.* (1994) is the only $^{40}Ar/^{39}Ar$ age from these eclogites which is characterized by a satisfactory plateau, we also consider this age suspect, because every other sample of these high-pressure rocks has yielded uninterpretable $^{40}Ar/^{39}Ar$ spectra (including the other two published by Searle *et al.*, 1994).

Recent studies have clearly shown that the $^{40}Ar/^{39}Ar$ data of white mica from high-pressure rocks are often contaminated with excess argon (e.g. Arnaud & Kelley, 1995; Ruffet *et al.*, 1995; Reddy *et al.*, 1996). U–Pb dating of zircon inclusions in garnet and Sm–Nd dating of garnet from the Dora Maira eclogite facies rocks (western Alps) both yielded Tertiary ages (e.g. Tilton *et al.*, 1991; Gebauer *et al.*, 1997) that cast doubt on the previously accepted Cretaceous $^{40}Ar/^{39}Ar$ plateau ages obtained for phengite from the same rocks (e.g. Hunziker *et al.*, 1989). Schermer *et al.* (1990), Tonarini *et al.* (1993) and Li *et al.* (1994) reported Rb–Sr ages on phengite from Mount Olympos blueschists, Greece, Himalayan eclogites, Pakistan, and Dabie Shan eclogites, China, that are younger than their corresponding $^{40}Ar/^{39}Ar$ ages, although the phengite closure temperature for $^{40}Ar/^{39}Ar$ is lower than that for Rb–Sr. These results underscore the need for the application of other geochronological techniques alongside $^{40}Ar/^{39}Ar$ dating for determining the ages of eclogites and blueschists, and making meaningful tectonic interpretations (e.g. Sherlock *et al.*, 1999).

In this paper, we present new whole-rock and mineral separate Rb–Sr data from the As-Sifah eclogite facies rocks in eastern Saih Hatat. We also present new $^{40}Ar/^{39}Ar$ data on phengite from the same samples, this time using replicate isothermal step heating to help remove or identify any possible excess Ar. This study is therefore aimed at: (i) constraining the age(s) of high-P/T metamorphism; (ii) providing insight into the cooling rates of these rocks; and (iii) presenting a revised tectonic model for the evolution of the Saih Hatat area in NE Oman.

GEOLOGICAL SETTING

The Saih Hatat area in NE Oman is a domal window that exposes basement, shelf and foreland basin units structurally beneath the allochthonous Semail ophiolite, Haybi Complex and Hawasina basin units (Glennie *et al.*, 1974; Fig. 1). The Saih Hatat basement consists of Proterozoic to Precambrian quartz–mica schists, metagreywackes and metabasites of the Hatat Formation and recrystallized dolomites of the Hijam Formation, unconformably overlain by Ordovician quartzites and metasiltstones of the Amdeh Formation (Glennie *et al.*, 1974; Le Métour *et al.*, 1986). The overlying shelf units consist of Permian to Lower Cretaceous metacarbonate rocks, interbedded with mafic, arenaceous and pelitic schists. Metamorphosed sandstones, conglomerates and a mélange overlie the shelf carbonates either unconformably or tectonically, and represent syntectonic foreland basin units, deposited shortly before the final stages of ophiolite emplacement in the Late Cretaceous (Muti Formation; Robertson, 1987a, b; El-Shazly, 1995; Fig. 1).

El-Shazly & Coleman (1990) subdivided the Saih Hatat area into three thrust-bounded regions based on the structural position of the lithostratigraphic units exposed in each area and variations in metamorphic grade (Fig. 1). After detailed mapping, Miller *et al.* (1999) identified the boundary between Regions II and III as a major ductile discontinuity separating two plates with different structural and metamorphic features. Their upper plate therefore includes imbricated, unmetamorphosed to weakly metamorphosed units, and corresponds to Regions I and II of El-Shazly & Coleman (1990), whereas their lower plate consists of strongly folded and deeply metamorphosed units, and corresponds to Region III (Fig. 1).

The units of Region I, located between Dar Sait and Hamiriya (the southern suburb of Ruwi) in northern Saih Hatat (Fig. 1), include unmetamorphosed Hawasina cherts, serpentinites and basalts, thrust onto a tectonic mélange (the Ruwi mélange). Following the interpretations of Le Métour *et al.* (1986) and Robertson (1987a, b), the Ruwi mélange is herein considered as the metamorphic equivalent of some members of the Muti Formation.

Region II consists of several thrust sheets of folded (parautochthonous) basement and shelf units (Precambrian to Early Cretaceous), metamorphosed under lawsonite–albite to epidote–blueschist facies conditions. These units exhibit a downsection increase in metamorphic grade (El-Shazly, 1994, 1995, 1996). In the northern parts of Region II, the Early Cretaceous units are missing, as the Ruwi mélange (Region I) is tectonically juxtaposed against Jurassic and Triassic units, all of which are deformed into a series of tight, overturned folds verging to the south or south-west. In the southern and western parts of Region II, the Hatat schists, Hijam dolomites, Amdeh quartzites and Saiq carbonates are deformed into large-scale overturned to recumbent open folds, and smaller scale cylindrical to sheath-like folds (Le Métour *et al.*, 1986; Gregory *et al.*, 1998; Miller *et al.*, 1999). A NE–SW-stretching lineation is well developed within the Hatat schists (Le Métour *et al.*, 1986; Michard *et al.*, 1994; Gregory *et al.*, 1998; Miller *et al.*, 1999). Miller *et al.* (1999) also report rare shear bands that record a top-to-the-NE transport direction in the deepest units of Region II.

Region III, the structurally lowest region, is more coherent, consisting of calcareous mica schists, metacarbonate rocks, mafic schists, metapelites and quartz–mica schists (Fig. 1). All of these units were considered by Le Métour *et al.* (1986) as part of the Permian Saiq Formation, although ^{13}C data do not support a Permian age for the protolith of some calcareous schists (Gregory *et al.*, 1998). An eastward increase in metamorphic grade and intensity of deformation led El-Shazly *et al.* (1990) to identify three metamorphic zones based primarily on mineral assemblages in mafic schists. In zone A, the mafic unit is characterized by greenschists, crossite–epidote schists and minor clinopyroxene-rich granofelses, interlayered on a centimetre to decimetre scale. In zone B, garnet–glaucophane schists are interlayered with glaucophane–epidote schists, clinopyroxene-rich granofelses and epidote amphibolites. Zone C is defined by the appearance of eclogites that are interlayered with garnet blueschists, clinopyroxene-rich granofelses and epidote–amphibolites (El-Shazly *et al.*, 1997). Peak conditions for this zone are estimated at 550–580 °C and 12–15 kbar (El-Shazly *et al.*, 1997; El-Shazly, 2001), although Wendt *et al.* (1993) and Searle & Cox (1999) favoured much higher pressures of 20 kbar for these rocks. A detailed description of the mineral assemblages of the different metamorphic zones of Region III was presented in El-Shazly *et al.* (1990), El-Shazly & Liou (1991), El-Shazly *et al.* (1997) and El-Shazly (2001).

The units of Region III experienced at least three deformational events (e.g. Searle *et al.*, 1994; Miller *et al.*, 1999). The earliest deformation resulted in a penetrative foliation that becomes layer

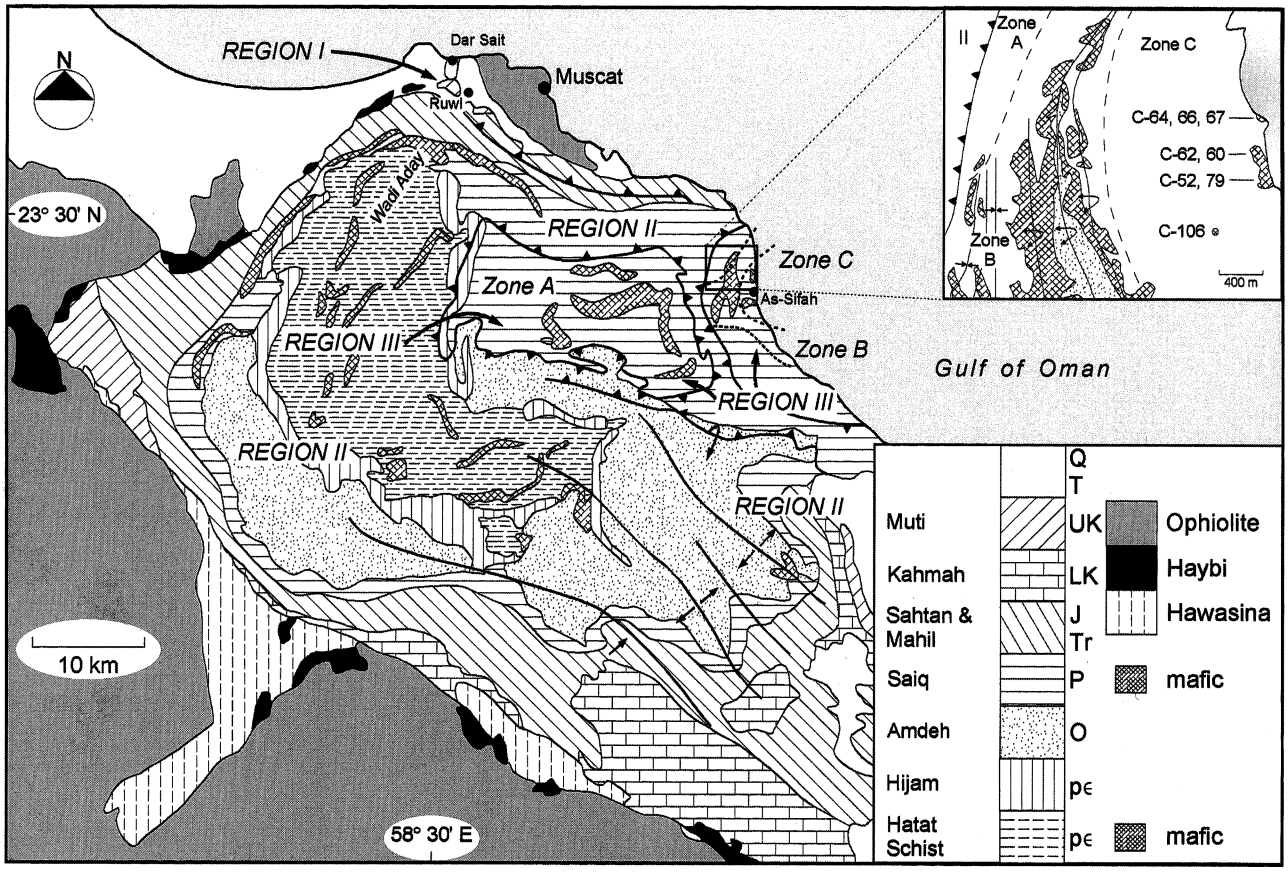

Fig. 1. Geological map of Saih Hatat, NE Oman, simplified after Le Métour *et al.* (1986) and Gregory *et al.* (1998). Regions I, II and III and metamorphic zones A, B and C are from El-Shazly & Coleman (1990) and El-Shazly *et al.* (1990). The key on the right represents the allochthonous units, whereas the key on the left represents the autochthonous and parautochthonous basement, shelf and foreland basin units. Q, Quaternary; T, Tertiary; K, Cretaceous; Tr, Triassic; J, Jurassic; P, Permian; pϵ, Precambrian. Inset: sample location map showing the mafic unit (hatched), quartz–mica schists (stippled) and calcareous schists (unpatterned). Note that most of the major structural boundaries shown here as thrusts have been reactivated as extensional shear zones during exhumation.

parallel in zones B and C, and is axial planar to later folds. The second deformational event (D2) produced the N to NE-vergent folds (which are inclined in zone A and become recumbent sheath folds in zone C), and which folded the D1 foliation. A NNE-trending lineation which plunges to the NNE or SSW (Michard *et al.*, 1984; Le Métour *et al.*, 1990; Gregory *et al.*, 1998) was also produced by D2. The third deformation (D3) took place under greenschist facies conditions and resulted in S–C and rotational fabrics and extensional crenulation cleavages (El-Shazly & Lanphere, 1992; Searle *et al.*, 1994; Miller *et al.*, 1999). A possible fourth deformational event is observed locally in zones B and C, and is manifested by broad, asymmetrical folds with E–W-striking axial planes, and a top-to-the-N? sense of shear. The development of late NW-striking, SW-dipping veins of $Qz \pm Cc \pm Hm \pm Ab \pm Ep \pm Chl$, typically with greenschist facies alteration halos cutting across lower plate units, marks a later brittle deformation. Localized, east-directed rockslides and falls represent the latest deformation and appear to be active to the present day.

SAMPLING, PETROGRAPHY AND MINERAL CHEMISTRY

Sample selection and analytical techniques

In this study, we focus on dating samples from the highest grade zone C of Region III. Ages obtained on eclogite facies rocks from this zone have so far been the most controversial. Moreover, constraining the ages of the highest grade metamorphic rocks in Saih Hatat is essential for tectonic interpretations. Seven samples collected from two coastal outcrops *c.* 1 km north of As-Sifah (Fig. 1) were selected for Rb–Sr and $^{40}Ar/^{39}Ar$ age dating after careful petrographic analysis with a polarizing microscope and, in some cases, microprobe analysis of the constituent minerals. These samples were collected from three distinct rock types interlayered on a decimetre scale: mafic blueschists, Cpx-rich granofelses and metasedimentary schists (Table 1). All layers are cofacial and have had identical *P–T* histories (cf. El-Shazly *et al.*, 1997). An eighth sample (C-106) of a boudinaged monomineralic vein of coarse-grained phengite cutting a retrogressed eclogite boudin was collected for $^{40}Ar/^{39}Ar$ dating from an outcrop *c.* 500 m west of the coastal outcrops. Unlike the rest of the samples, this vein is likely to have formed during the early stage of exhumation of the blueschists and eclogites of zone C.

The seven eclogite facies samples were crushed and sieved, and phengite was separated from the 500–1000 μm size fraction using an isodynamic separator at Sultan Qaboos University, shaking on filter paper, and hand-picking under a binocular microscope. An additional aliquot of phengite was separated from the 250–500 μm size fraction for samples C-64, C-52 and C-62 to investigate the effect of grain size on the $^{40}Ar/^{39}Ar$ age spectra. Crystals with inclusions were eliminated, and all separates were optically homogeneous. Each separate was divided into three aliquots: two for Rb–Sr and $^{40}Ar/^{39}Ar$ dating, and the third for scanning electron microscopy (SEM)

imaging and analysis. The aliquot used for Rb–Sr dating was further cleaned by grinding in ethanol using an agate mortar, and washing in ethanol (*P*.a.) and H_2O (three times distilled) in an ultrasonic bath. The aliquot used for SEM analysis was mounted on a glass slide with epoxy, polished, carbon coated and analysed using a JEOL 840A scanning electron microscope at Sultan Qaboos University. Details of standardization and analysis are described in El-Shazly (2001).

Petrography and mineral chemistry

Mineral assemblages are listed in Table 1. Samples C-52 and C-67 are mafic blueschists consisting of predominantly Gln + Ep + Ph, with smaller amounts of Cpx ± Gt. In both samples, glaucophane and epidote are in textural equilibrium with phengite, but appear to have crystallized after (and possibly at the expense of) Gt ± Cpx. Retrograde phases include Ab + Cc + Chl ± Win ± Bt, and are more common in C-52 (Table 1). Phengite occurs as fine- to medium-grained crystals (0.4–2 mm long) that define the foliation. The crystals are not kinked, and appear to have been partially polygonized during D2. Phengite contains numerous inclusions of rutile, and rare inclusions of Hm ± Ttn ± Ep. In C-52, the phengite crystals are significantly fractured, with some fractures filled with albite, chlorite and winchite. Phengite from C-52 is irregularly but weakly zoned (Fig. 2a), with both separated size fractions having the same composition and zoning. In C-67, phengite crystals are regularly zoned from Si- and Mg-rich cores (Si = 3.40–3.62 atoms per formula unit (apfu), calculated on the basis of 11 oxygens; Fe/Mg = 0.47–0.56) to less siliceous rims (Si = 3.30 apfu; Fe/Mg = 0.62–0.88; Table 2).

Samples C-60 and C-64 were collected from eclogitic Cpx-rich layers. Both samples are characterized by a weak foliation defined by the orientation of Cpx ± Ph, and are pristine, containing only traces of retrograde albite, winchite, chlorite ± biotite (Table 1). Phengite occurs as fine- to medium-grained (0.6–2 mm) subidioblastic crystals which appear to have crystallized after garnet and Cpx, often in garnet pressure shadows. In C-60, phengite is almost devoid of inclusions, and is regularly zoned from Si- and Mg-rich cores (Si = 3.60 apfu, Fe/Mg = 0.4) to less siliceous, more ferroan rims (Si = 3.38 apfu, Fe/Mg = 0.5–0.9; Table 2). In C-64, phengite crystals are more fractured and contain several inclusions of Cpx and rutile, and are sometimes partially rimmed by albite. The zoning patterns are more irregular, although they show an overall trend of decreasing Si and increasing Fe/Mg from core to rim (Fig. 2b; Table 2). Different size fractions of phengite from this sample have similar compositions and zoning patterns.

Samples C-62, C-66 and C-79 were all collected from metasedimentary schists which contain $\geq$ 30 vol.% phengite, as well as significant amounts of garnet and glaucophane (Table 1). These rocks differ from the Na- and Fe-rich metapelites described by El-Shazly & Liou (1991), as they lack paragonite and chloritoid (Table 1). Their most likely protolith is a mixture of mafic to intermediate tuffs and mudstones. Sample C-79 is pristine, and almost devoid of any signs of retrogression. Sample C-66 shows a few retrograde features such as glaucophane and Cpx partially replaced by oxychlorite and calcite. On the other hand, C-62 was significantly affected by retrogression where garnet is partially replaced by phengite, epidote, glaucophane, albite and chlorite along fractures and rims, and symplectites of albite + sodic–calcic amphibole (replacing Cpx?) are common. Phengites are medium-grained (1.5–2 mm), subidioblastic crystals that define the foliation and are devoid of kink bands. In C-66 and C-79, phengite contains a few inclusions of rutile (± minor garnet), very few fractures and is regularly zoned from Si- and Mg-rich cores to less siliceous rims with higher Fe/Mg (Fig. 2c; Table 2). In C-62, the phengite is complexly and irregularly zoned, has a higher density of fractures and is occasionally rimmed by chlorite (Table 2). There are no chemical differences between the different size fractions of phengite separated from this sample.

Phengite of sample C-106 is very coarse grained (1–2 cm long). It is almost chemically homogeneous with Si = 3.53–3.56 apfu and the lowest Fe/Mg ratios (0.17–0.45) in all dated samples (Table 2). It has very few fractures, but contains many inclusions of albite, biotite, chlorite, rutile and winchite near its rims.

$^{40}Ar/^{39}Ar$ DATING

Analytical techniques

Phengite separates were wrapped in Cu foil, sealed in a quartz vial and irradiated at the TRIGA reactor at Oregon State University for 16 MWh. Ratios of reactor-produced Ca-derived isotopes were established by analysing CaF_2 included in the irradiation vial. Sanidine from the Fish Canyon tuff, with a preferred age of 27.8 Ma, was used as a neutron flux monitor. The monitor packets were interspersed between every six unknown packets; *c*. 0.8 mg of each monitor was analysed with the resistance furnace to determine irradiation parameter, *J*. We used an uncertainty of 0.2% (at 1σ) for *J* for all samples.

All samples, which are multigrain splits of small mass (*c*. 1 mg), were analysed over a two-week period using a double-vacuum Staudacher-type resistance furnace. To improve upon previous efforts at dating phengite, and in an attempt to resolve the influence of excess Ar and complications in spectral interpretation, we performed a large number of isothermal heating steps. Each cycle comprised 2 min of heating from 300 °C to the set temperature, 5–90 min (most commonly 10 min) of constant temperature, and 3 min cooling to 300 °C. Gas was gettered continuously during extraction with two SAES ST172 Zr–V–Fe getters operated at 4 A and 2 A. The collected gas was analysed for 7–9 min in an MAP-216 spectrometer with a Baur–Signer source and Johnston MM1 electron multiplier operating in static mode with a room temperature SAES ST707 Zr–V–Fe getter. Peak heights at the time of gas introduction into the mass spectrometer were determined by extrapolating the evolved signal size using a linear regression. The mass discrimination, determined by analysing the $^{40}Ar/^{36}Ar$ ratio of air, was 0.993 per atomic mass unit (a.m.u.) during the course of these experiments. Resistance furnace *m/e* 40 blanks varied from 2.9×10^{-16} mol at 800 °C to 1.2×10^{-15} mol at 1400 °C.

Table 1. Modal contents of samples dated[a].

Sample	Gt	Cpx	Gln	Ep	Ph	Chl	Ab	Qz	Opq	Rt	Others
Mafic blueschists											
C-52	5	3	15–20	30	10–15	5–7	15	2	2	tr	Cc(10), Win(2), Ttn(tr)
C-67	—	20	20–25	20–25	15	3–5	3–5	—	7–10	2–3	Cc(3–5), Bt(tr)
Cpx-rich											
C-60	10–12	50–60	5	3	15	tr	tr	3–5	2–3	1	Ap(tr)
C-64	20–25	45–50	3	Aln(3)	7–10	1–2	tr	7–10	Mgt(1–2)	tr	Bt(tr)
Metasedimentary schists											
C-62	10–15	tr	20	2	30	5–7	7–10	2–3	7–10	tr	Cc(2–3), Aln(tr), Win(2)
C-66	1–2	7–10	10–15	2–3	55–60	5	3	5	3	—	Cc(5), Ap(tr)
C-79	15–20	2–3	20–25	2–3	30	3–5	—	5	1–2	2	Cc(15–20), Bt(tr)

[a]Modal contents estimated visually.
tr, traces.

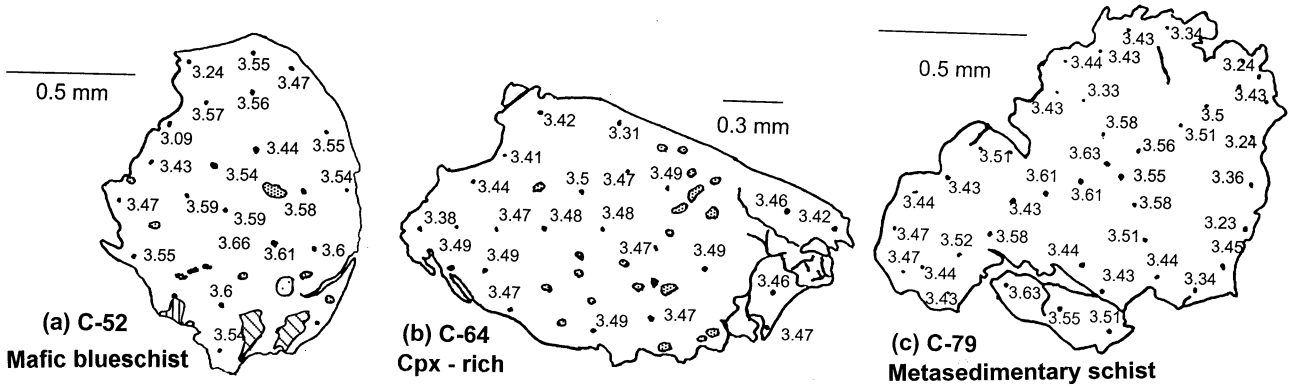

Fig. 2. Sketches of representative phengite grains from samples (a) C-52 (grain 1), (b) C-64 (grain 8) and (c) C-79 (grain 4), showing their Si contents in atoms per formula unit calculated on the basis of 11 oxygen atoms. Densely stippled grains, inclusions of rutile; light stipple, titanite; diagonal rules, chlorite; vertical rules, epidote.

Results

The spectra obtained for all samples are characterized by K/Ca (>0.04) and K/Cl ratios that are within the normal range for K-white mica, suggesting that the separates are indeed pure. Nevertheless, these samples yield complex spectra with different shapes and total gas ages that range from 148 to 84.9 Ma (Table 3). The simplest spectrum, aliquot C-62f, decreases from low-T steps at *c*. 95 Ma to high-T steps at *c*. 92 Ma. The coarser grained aliquot of this sample, C-62c, yields a weakly hump-shaped spectrum from 96 to 92 Ma. Samples C-64, C-66 and C-106 all yield the oldest apparent ages in their lowest and highest temperature steps. Apparent ages given by the intermediate temperature steps increase gradually to some peak value before dropping once more, giving rise to a 'W'- or saddle-shaped spectrum with an intermediate hump (Figs 3 & 4). The spectrum for C-67 is overall saddle-shaped with some irregularities (Fig. 5); 45% of the gas defines a plateau age of *c*. 100 Ma. Samples C-52 (Fig. 5), C-60 (Fig. 3) and C-79 (Fig. 4) yield hump-shaped spectra with several irregularities.

In the three samples where two aliquots of different grain sizes were dated, the finer grained size fractions always yielded slightly younger apparent total gas ages (Table 3). Extensive isochron analysis does not reveal systematic behaviour for any of the spectra, and we

Table 2. Representative analyses of phengite.

	C-52				C-60		C-62		C-64						C-66					C-79				C-67				C-106			
Sample	1				6		1		4		7		1		1		2		2	2c		4		2						
Grain	8	9	11	21	1	3	1	8	5	14	1	2	2	3	4	1	4	5	11	20	7	1	7	5	16	19	22				
Analysis	c	r	c	r	c	r	r	c	c	r	c	r	c	r	c	r	c	r	r	c	r	r	c	c	r	r	ir	c	ir	or	
SiO_2	53.25	53.61	54.23	53.97	52.72	51.50	51.32	50.57	53.49	50.69	51.88	50.91	51.29	51.85	52.33	52.34	52.81	52.08	49.78	50.80	52.92	51.59	51.95	51.96	48.92	49.53	50.78	54.05	53.16	50.35	
TiO_2	0.27	0.25	0.17	0.18	0.16	0.20	0.23	0.23	0.21	0.25	0.20	0.33	0.26	0.31	0.21	0.29	0.25	0.29	0.28	0.15	0.26	0.43	0.25	0.17	0.37	0.35	0.30	0.19	0.32	0.22	
Al_2O_3	23.51	24.25	22.47	24.14	20.61	22.34	23.09	22.36	22.56	24.62	23.30	23.73	23.70	23.45	19.73	23.46	21.07	22.20	25.89	23.91	21.08	24.86	19.93	20.53	26.50	26.75	23.33	22.46	21.43	21.52	
Cr_2O_3	0.00	0.00	0.01	0.00	0.00	0.00	0.10	0.00	0.01	0.00	0.06	0.05	0.00	0.00	0.03	0.03	0.04	0.00	0.03	0.06	0.06	0.01	0.09	0.15	0.13	0.14	0.00	0.11	0.08	0.13	
FeO	2.66	2.78	2.29	2.80	3.76	3.67	4.66	4.56	4.76	4.46	3.74	3.64	3.91	3.90	5.87	4.32	5.52	4.76	4.66	4.59	4.85	4.40	4.84	4.44	4.34	3.95	4.52	2.42	2.54	5.68	
MnO	0.00	0.04	0.00	0.00	0.05	0.03	0.00	0.03	0.00	0.00	0.00	0.47	0.00	0.04	0.01	0.05	0.01	0.01	0.00	0.03	0.00	0.03	0.00	0.00	0.02	0.06	0.06	0.00	0.00	0.00	
MgO	4.62	4.43	5.00	4.47	4.99	4.69	3.76	3.76	4.08	3.23	4.25	4.02	4.09	4.19	4.41	4.12	4.26	4.17	2.85	4.24	4.44	4.23	4.83	4.99	2.90	2.78	4.10	5.31	5.27	6.96	
Na_2O	0.44	0.42	0.35	0.45	0.28	0.40	0.33	0.26	0.30	0.46	0.38	0.42	0.42	0.36	0.27	0.34	0.19	0.37	0.68	0.42	0.28	0.37	0.20	0.35	0.91	0.92	0.47	0.31	0.26	0.20	
K_2O	10.88	10.76	10.75	10.82	10.84	10.92	10.93	10.79	11.29	10.58	11.16	11.35	11.29	11.38	11.06	11.00	11.51	11.05	10.43	10.86	11.29	10.89	11.30	11.04	10.59	10.53	11.16	11.41	11.16	9.56	
Total	95.63	96.54	95.28	96.83	93.42	93.75	94.42	92.57	96.70	94.30	94.98	94.91	94.96	95.48	93.93	95.95	95.65	94.93	94.60	95.06	95.19	96.81	93.39	93.63	94.68	95.01	94.72	96.25	94.22	94.62	
Si	3.55	3.54	3.61	3.55	3.63	3.54	3.51	3.53	3.57	3.47	3.53	3.47	3.49	3.51	3.63	3.51	3.59	3.55	3.40	3.46	3.60	3.44	3.61	3.59	3.34	3.36	3.47	3.59	3.61	3.45	
Al^{IV}	0.43	0.45	0.38	0.44	0.37	0.45	0.48	0.46	0.42	0.52	0.46	0.51	0.49	0.48	0.36	0.47	0.40	0.44	0.59	0.54	0.39	0.54	0.38	0.40	0.64	0.62	0.51	0.40	0.37	0.54	
Ti	0.01	0.01	0.01	0.01	0.01	0.01	0.01	0.01	0.01	0.01	0.01	0.02	0.01	0.02	0.01	0.01	0.01	0.01	0.01	0.01	0.01	0.02	0.01	0.01	0.02	0.02	0.02	0.01	0.02	0.01	
Al(total)	1.85	1.89	1.77	1.87	1.67	1.81	1.86	1.84	1.78	1.98	1.87	1.91	1.90	1.87	1.61	1.86	1.69	1.78	2.08	1.92	1.69	1.95	1.63	1.67	2.13	2.14	1.88	1.76	1.72	1.74	
Al^{VI}	1.41	1.44	1.39	1.43	1.31	1.36	1.39	1.38	1.36	1.46	1.40	1.39	1.41	1.39	1.25	1.39	1.29	1.35	1.50	1.38	1.30	1.41	1.25	1.27	1.49	1.52	1.37	1.36	1.35	1.20	
Cr	0.00	0.00	0.00	0.00	0.00	0.00	0.01	0.00	0.00	0.00	0.00	0.00	0.00	0.00	0.00	0.00	0.00	0.00	0.00	0.00	0.00	0.00	0.00	0.01	0.01	0.01	0.00	0.01	0.00	0.01	
Fe	0.15	0.15	0.13	0.15	0.22	0.21	0.27	0.27	0.27	0.26	0.21	0.21	0.22	0.22	0.34	0.24	0.31	0.27	0.27	0.26	0.28	0.25	0.28	0.26	0.25	0.22	0.26	0.13	0.14	0.33	
Mn	0.00	0.00	0.00	0.00	0.00	0.00	0.00	0.00	0.00	0.00	0.00	0.03	0.00	0.00	0.00	0.00	0.00	0.00	0.00	0.00	0.00	0.00	0.00	0.00	0.00	0.00	0.00	0.00	0.00	0.00	
Mg	0.46	0.44	0.50	0.44	0.51	0.48	0.38	0.39	0.41	0.33	0.43	0.41	0.41	0.42	0.46	0.41	0.43	0.42	0.29	0.43	0.45	0.42	0.50	0.51	0.30	0.28	0.42	0.53	0.53	0.71	
Na	0.06	0.05	0.05	0.06	0.04	0.05	0.04	0.04	0.04	0.06	0.05	0.06	0.06	0.05	0.04	0.04	0.03	0.05	0.09	0.06	0.04	0.05	0.03	0.05	0.12	0.12	0.06	0.04	0.03	0.03	
K	0.93	0.91	0.91	0.91	0.95	0.96	0.95	0.96	0.96	0.92	0.97	0.99	0.98	0.98	0.98	0.94	1.00	0.96	0.91	0.94	0.98	0.93	1.00	0.97	0.92	0.91	0.97	0.97	0.97	0.84	
Oct total	2.02	2.03	2.01	2.02	2.04	2.05	2.04	2.04	2.03	2.05	2.05	2.04	2.04	2.04	2.05	2.05	2.04	2.04	2.05	2.08	2.03	2.08	2.03	2.05	2.05	2.03	2.05	2.02	2.03	2.25	
Fe/Mg	0.32	0.35	0.26	0.35	0.42	0.44	0.70	0.68	0.65	0.78	0.49	0.51	0.54	0.52	0.75	0.59	0.73	0.64	0.92	0.61	0.61	0.60	0.56	0.51	0.83	0.79	0.62	0.26	0.27	0.46	

c, core; r, rim; ir, inner rim; or, outer rim.

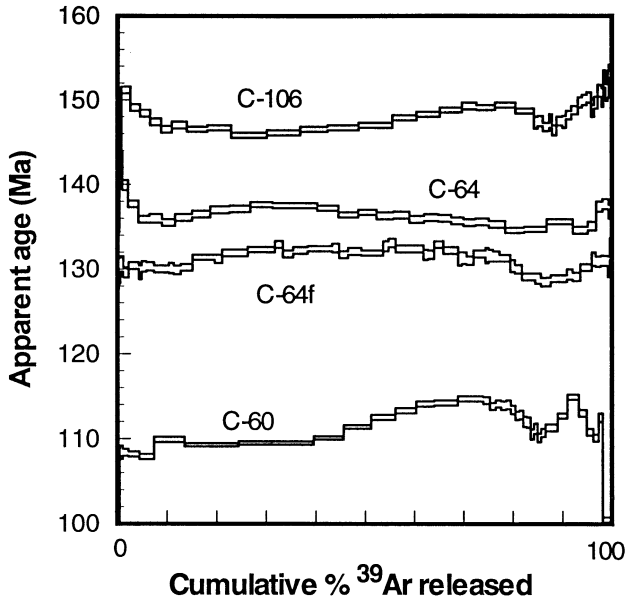

Fig. 3. $^{40}Ar/^{39}Ar$ age spectra for phengite from Cpx-rich samples C-60, C-64 and vein C-106. C-64f is the finer grained aliquot of sample C-64.

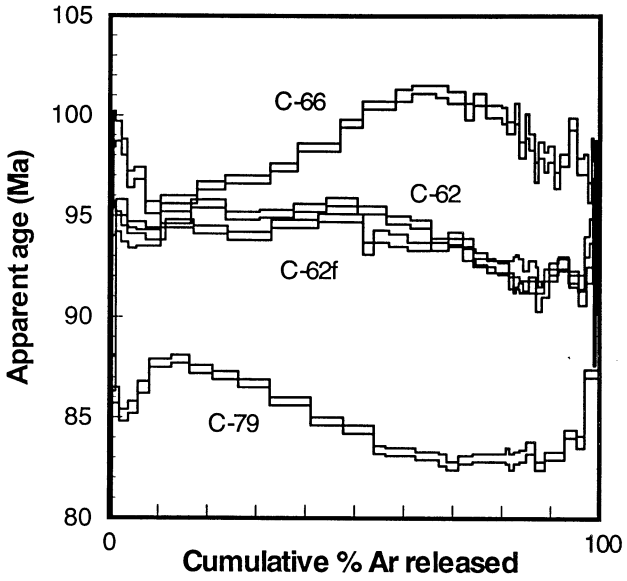

Fig. 4. $^{40}Ar/^{39}Ar$ age spectra for phengite from metasedimentary samples C-62, C-66 and C-79. C-62f is the finer grained aliquot of sample C-62.

interpret the lowest ages in each spectrum to be a maximum age for the sample.

Rb–Sr DATING

Analytical techniques

Isotope analyses were carried out at the Zentrallaboratorium für Geochronologie at the Institut für Mineralogie, Universität Münster, using a VG Sector 54 multicollector mass spectrometer (Sr) and an NBS-type Teledyne mass spectrometer (Rb). For Rb–Sr analyses, whole-rock powders (about 100 mg) and mineral separates (phengite, *c.* 24–43 mg; epidote, *c.* 3–5 mg; omphacite, *c.* 95 mg) were mixed with an ^{87}Rb–^{84}Sr spike in Teflon screw-top vials and dissolved in an HF–HNO_3 (5 : 1) mixture on a hot plate overnight. After drying, 6 N HCl was added to the residue. This mixture was homogenized on a hot plate overnight. After a second evaporation to dryness, Rb and Sr were separated by standard ion-exchange procedures (AG 50W-X8 resin) on quartz glass columns using 2.5 N and 6 N HCl as eluents. For mass spectrometric analysis, Rb and Sr were loaded on Ta filaments with H_2O and H_3PO_4, respectively. Correction for mass fractionation is based on an $^{86}Sr/^{88}Sr$ ratio of 0.1194. Rb ratios were corrected for mass fractionation using a factor deduced from multiple measurements of Rb standard NBS 607. Total procedural blanks were < 0.1 ng for Rb and < 0.15 ng for Sr. Based on repeated measurements, the $^{87}Rb/^{86}Sr$ ratios were assigned an uncertainty of 1% (2σ). For other isotope ratios, uncertainties are reported at the $2\sigma_m$ level. Repeated runs of NBS standard 987 gave an average $^{87}Sr/^{86}Sr$ ratio of 0.710265 ± 24 (2σ, $n = 41$). All ages and elemental concentrations were calculated using the IUGS recommended decay constants (Steiger & Jäger, 1977). Rb–Sr ages were calculated using the least-squares regression technique of York (1969). Ages and errors are reported at the 2σ level. The Rb–Sr isotopic data are summarized in Table 4.

Results

Two-point isochrons using phengite–whole rock, phengite–epidote or phengite–clinopyroxene yield ages between 77.8 ± 1.2 and 77.2 ± 0.8 Ma for all mafic blueschist and metasedimentary schist samples (Table 4). Isochrons for the Cpx-rich samples (C-60 & C-64) yield slightly older ages of 79.2 ± 0.8 and 78.6 ± 0.9 Ma, respectively (Fig. 6; Table 4).

Table 3. Summary of results of $^{40}Ar/^{39}Ar$ dating of phengite.

Sample	Size fraction (μm)	J	Total gas age (Ma)	Preferred age (Ma)	Shape of spectrum
C-52f	250–500	0.0039992	125	≤ 108	Hump
C-52	500–1000	0.0039699	131	≤ 115	Hump
C-67	500–1000	0.0040127	99.4	≤ 96	Saddle + hump
C-60	500–1000	0.0040022	111	≤ 108	Hump
C-64f	250–500	0.0039898	131	≤ 130	Hump
C-64	500–1000	0.0039962	136	≤ 133	Saddle + hump
C-62f	250–500	0.0039724	93.6	≤ 92	Irregular
C-62	500–1000	0.0040090	94.1	≤ 92	Irregular
C-66	500–1000	0.0039930	98.4	≤ 96	Saddle + hump
C-79	500–1000	0.0039785	84.9	≤ 83	Hump
C-106	> 1 cm	0.0039865	148	≤ 146	Saddle

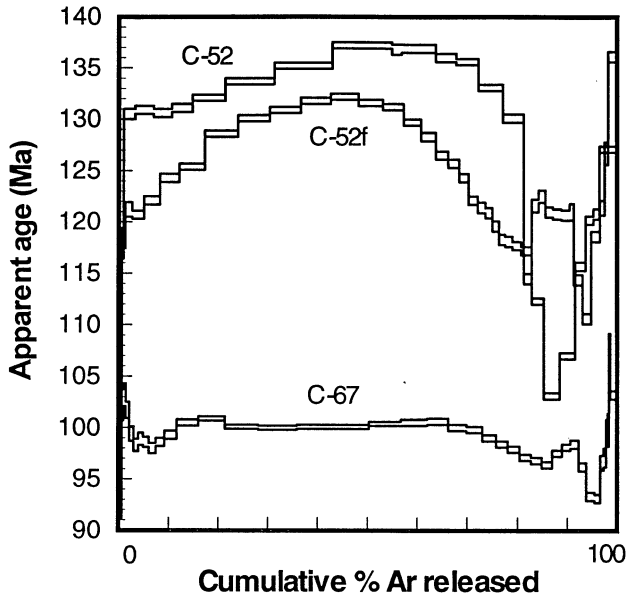

Fig. 5. $^{40}Ar/^{39}Ar$ age spectra for phengite from mafic samples C-67 and C-52. C-52f is the finer grained aliquot of sample C-52.

$(^{87}Sr/^{86}Sr)_i$ ratios range from 0.709 to 0.714, and show no correlation with rock type or extent of retrogression. Whole-rock Rb values for the dated samples range from 17.49 to 190 ppm, whereas the $^{87}Rb/^{86}Sr$ ratios range from 0.4 to 12.58 (Table 4).

INTERPRETATION OF THE AGE DATA

The Rb–Sr ages defined by two-point isochrons are similar for all samples, regardless of the lithology or the extent of retrogression of the dated samples. On the other hand, the $^{40}Ar/^{39}Ar$ age spectra are all perturbed, with different samples yielding different total gas ages. As in the case of the Rb–Sr ages, there is no relationship between the apparent $^{40}Ar/^{39}Ar$ ages yielded by each phengite separate and the rock type or its extent of retrogression. There is also no clear relationship between the chemistry of the phengite (e.g. the Si contents, zoning patterns or Fe/Mg ratios) and the apparent ages (cf. Scaillet *et al.*, 1992).

Given that the ideal closure temperature for Rb–Sr in phengite (*c.* 500 ± 50 °C; Purdy & Jäger, 1976; Blanckenburg *et al.*, 1989) is higher than that for Ar in the same mineral (350–430 °C; e.g. Purdy & Jäger, 1976; Sisson & Onstott, 1986; Blanckenburg *et al.*, 1989; Kirschner *et al.*, 1996), the $^{40}Ar/^{39}Ar$ ages are expected to be younger than the Rb–Sr ages for the same sample. However, the Rb–Sr ages (78.2 ± 2 Ma) are considerably younger than any of our $^{40}Ar/^{39}Ar$ ages (146–83 Ma). This could have three possible explanations.

1 The $^{40}Ar/^{39}Ar$ ages approximate the age of the high-*P*/*T* peak metamorphism, whereas the 78 ± 2 Ma age represents a second metamorphic event that caused the resetting of the Rb–Sr system and the perturbation of the $^{40}Ar/^{39}Ar$ spectra.

2 The younger Rb–Sr ages result from the mobilization of Sr by fluids during retrogression, and its subsequent loss from the dated minerals, whereas Ar, being an inert gas, was unaffected by these retrogressive fluids.

3 The Rb–Sr ages of 78 ± 2 Ma represent the time at which the As-Sifah eclogite facies rocks cooled through 500 ± 50 °C, whereas the $^{40}Ar/^{39}Ar$ ages of ≥ 83 Ma can only be considered maximum ages of peak metamorphism, as this phengite has incorporated excess Ar.

It is unlikely that the observed difference in $^{40}Ar/^{39}Ar$ and Rb–Sr ages is representative of two metamorphic events, because the closure temperature of phengite for Sr is higher than that for ^{40}Ar (e.g. Purdy & Jäger, 1976; Blanckenburg *et al.*, 1989). Loss of Sr from phengite during retrogression is also an unlikely explanation, simply because different samples with different degrees of retrogression (e.g. C-79 & C-62) yield the same Rb–Sr ages. Therefore, the most plausible explanation for the age difference is that the Rb–Sr ages record cooling shortly after a period of extensive crystallization close to 78 ± 2 Ma, whereas the $^{40}Ar/^{39}Ar$ ages are not meaningful because of the incorporation of excess Ar in phengite.

This conclusion is supported by several observations.

1 There is large variability in $^{40}Ar/^{39}Ar$ spectral shapes and total gas ages from samples with identical *P*–*T* histories.

2 The oldest apparent $^{40}Ar/^{39}Ar$ age is recorded by C-106 phengite. However, this sample is younger than all other eclogitic phengite, as it formed during retrogression and veining.

3 Different grain size separates from the same sample yield different $^{40}Ar/^{39}Ar$ ages. The fact that the coarser aliquots yield older ages leads us to conclude that

Table 4. Results of Rb–Sr dating.

Sample	Type	Rb (ppm)	Sr (ppm)	$^{87}Rb/^{86}Sr$[a]	$^{87}Sr/^{86}Sr$	Error[b]	Age (Ma)
C-52	Whole rock	17.49	126.3	0.401	0.713691	22	
C-52	*Epidote*[c]	4.585	466.7	0.028	0.713386	24	77.2 ± 0.8
C-52	*Phengite*	274.0	6.769	118.651	0.843512	33	
C-67	Whole rock	48.43	52.99	2.645	0.712511	23	
C-67	*Epidote*	2.575	870.0	0.0086	0.711909	22	77.6 ± 0.8
C-67	*Phengite*	432.9	9.575	132.750	0.858253	27	
C-60	*Whole rock*	94.08	25.36	10.747	0.720569	21	78.6 ± 0.9
C-60	*Phengite*	397.9	14.13	82.21	0.800357	34	
C-64	Whole rock	21.52	58.50	1.064	0.711774	24	
C-64	*Omphacite*	2.835	18.42	0.445	0.710679	22	79.2 ± 0.8
C-64	*Phengite*	287.9	10.38	80.982	0.801284	27	
C-62	Whole rock	137.3	39.26	10.128	0.720599	21	
C-62	*Epidote*	1.771	565.2	0.0091	0.710344	21	77.6 ± 0.8
C-62	*Phengite*	593.1	8.181	214.640	0.947072	41	
C-66	*Whole rock*	190.3	43.81	12.587	0.723770	24	77.8 ± 1.2
C-66	*Phengite*	430.5	8.793	143.899	0.868834	39	
C-79	Whole rock	150.3	49.31	8.830	0.722599	20	
C-79	*Epidote*	3.413	614.4	0.016	0.713796	20	77.4 ± 0.8
C-79	*Phengite*	336.1	3.305	303.985	1.047872	44	

[a]The $^{87}Rb/^{86}Sr$ ratios were assigned uncertainties of 1% 2σ.
[b]Values indicate uncertainties in the last two digits of the $^{87}Sr/^{86}Sr$ ratios quoted at the $2\sigma_m$ level.
[c]Italics indicate phases used for age calculation.

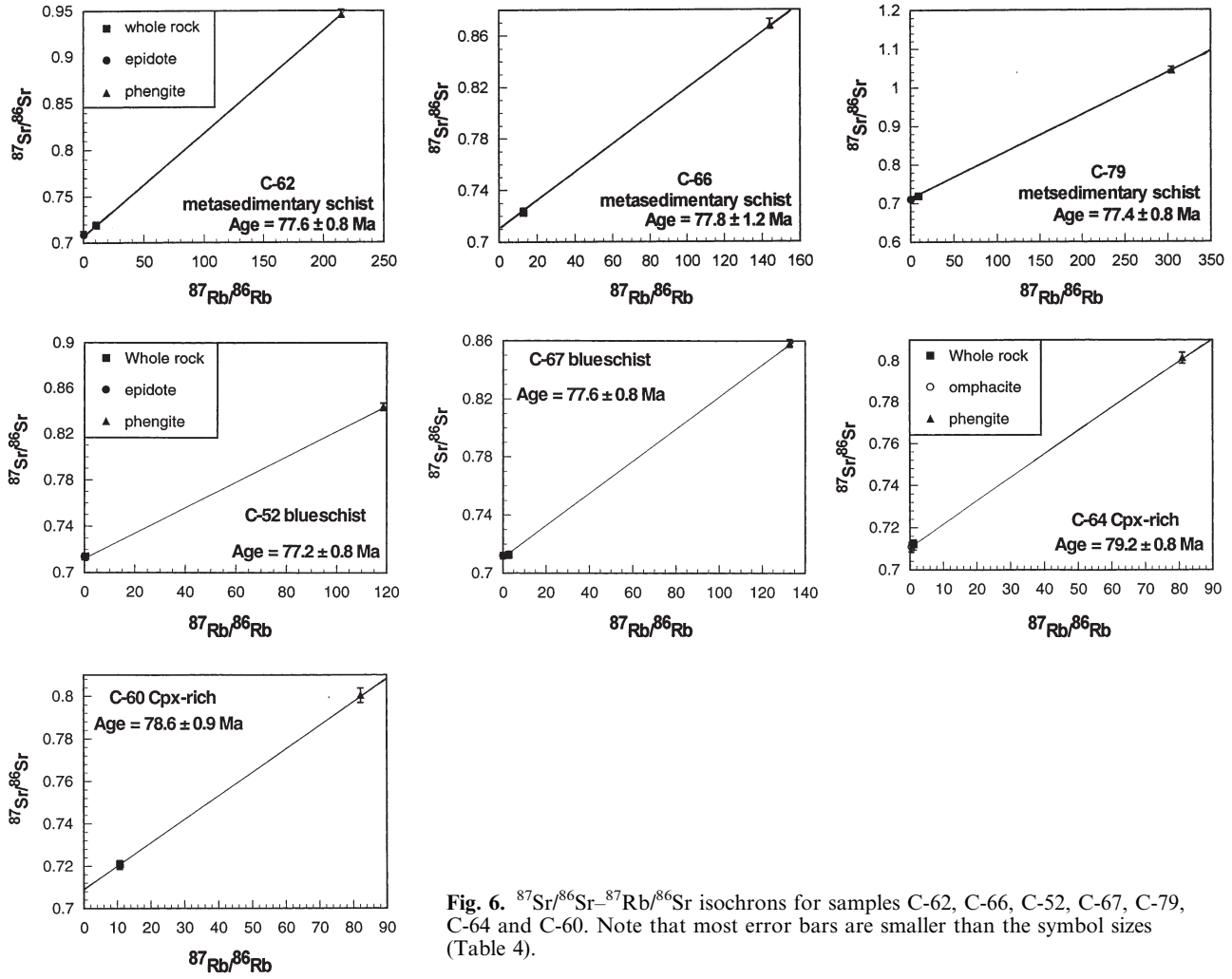

Fig. 6. $^{87}Sr/^{86}Sr$–$^{87}Rb/^{86}Sr$ isochrons for samples C-62, C-66, C-52, C-67, C-79, C-64 and C-60. Note that most error bars are smaller than the symbol sizes (Table 4).

excess Ar was added before the most recent Ar loss event. If the phengite underwent a growth event or complete recrystallization such that all Ar was lost and then the excess Ar was added diffusively to the crystals, the finer grained samples would have been most affected and would have yielded the oldest apparent ages, which is not the case.

4 Saddle-shaped $^{40}Ar/^{39}Ar$ spectra, similar to those of C-67, C-64 and C-106, are considered to be indicative of the presence of excess Ar (Lanphere & Dalrymple, 1976; McDougall & Harrison, 1988). Although more difficult to interpret, hump-shaped spectra, similar to those of C-52, C-60 and C-79, have also been attributed to excess Ar (e.g. Hannula & McWilliams, 1995). Other interpretations of hump-shaped spectra as dating a mixture of two populations of white mica with different ages (Wijbrans & McDougall, 1986), partial re-equilibration of celadonite-rich phengite under lower pressure during exhumation (Scaillet *et al.*, 1992) and subgrain chemical heterogeneity (Hammerschmidt & Franz, 1992) are less likely because, for all samples (except C-62), our separates consist of a single generation of phengite, and there is no relation between the extent of sample retrogression or zoning patterns of these micas and their resulting age spectra.

5 Phengite with a higher density of fractures (e.g. C-64 & C-52) yields older apparent ages compared to that from less fractured crystals. This is consistent with the incorporation of excess Ar, a significant component of some metamorphic fluids (e.g. Cumbest *et al.*, 1994), via fractures in phengite (e.g. Reddy *et al.*, 1996).

The results of this study are not unique. Dallmeyer *et al.* (1990) reported variably discordant $^{40}Ar/^{39}Ar$ age spectra for phengite from blueschists and eclogites from west-central Spitsbergen that yielded slightly older ages compared to those obtained from Rb–Sr phengite–whole-rock isochrons. Tonarini *et al.* (1993) reported $^{40}Ar/^{39}Ar$ plateau ages for phengite that were considerably older than Sm–Nd and Rb–Sr isochron ages for eclogites from the Himalayas. Li *et al.* (1994) and Inger *et al.* (1996) also reported much older $^{40}Ar/^{39}Ar$ ages than corresponding Rb–Sr phengite

ages from Dabie Shan, China and the Sesia Lanzo eclogites, western Alps, respectively. Bröcker & Franz (1998) and Sherlock *et al.* (1999) reported younger Rb–Sr ages for blueschist facies phengite compared to their corresponding $^{40}Ar/^{39}Ar$ ages for samples from the intermediate unit of Tinos, Cyclades, and the Tavsanli zone, north-west Turkey, respectively. Along with the results of Tilton *et al.* (1991) and Gebauer *et al.* (1997) on Dora Maira eclogites, it seems that excess Ar is common in high-pressure phengite. The amount of excess Ar apparently increases with increased access to fluids and increasing metamorphic pressures (e.g. Sherlock *et al.*, 1999).

TECTONIC SYNTHESIS

The success of any tectonic model for the formation and exhumation of the high-*P*/*T* metamorphic rocks of Saih Hatat is gauged by its ability to account for the stratigraphic, geochronological, petrological, cooling rate and structural data available for this area. More than 10 different models have been proposed for the tectonic evolution of Saih Hatat. The principal differences among these models pertain to the timing of high-*P*/*T* metamorphism and the peak pressures attained by the blueschists and eclogites. Our position on these two issues is as follows.

1 Phengite from high-pressure rocks is commonly contaminated with excess Ar (e.g. Sherlock *et al.*, 1999). The geological significance of $^{40}Ar/^{39}Ar$ ages for phengite should be considered suspect unless supported by age data obtained using other geochronological techniques.

2 Pressures estimated for the As-Sifah high-*P*/*T* rocks using empirical geobarometers or thermodynamic calculations of pressure-sensitive equilibria should be considered suspect unless they are consistent with the *P*–*T* stability ranges of the mineral assemblages in these rocks and all interlayered cofacial lithologies.

The data most relevant to constraining the tectonic evolution of NE Oman are listed below.

Stratigraphic and geochronological constraints

1 The garnet blueschists and epidote amphibolites of zone C appear to have the same protoliths as the crossite–epidote schists and greenschists of zone A, as indicated by the geochemical data of El-Shazly *et al.* (1994, 1997). The persistent occurrence of Cpx-rich granofels within the mafic unit, as well as layers of quartz–mica schists, metapelites and calcareous mica schists in all three metamorphic zones, suggests that the same units occur throughout Region III, and were folded, boudinaged and metamorphosed under different *P*–*T* conditions in the different zones. Whether the protoliths of these rocks are pre-Permian (e.g. Glennie *et al.*, 1974) or Permian (Le Métour *et al.*, 1986), they represent an integral part of the continental basement or shelf of Oman. The suggestions of Michard *et al.* (1994) and Searle *et al.* (1994) that the As-Sifah units represent a terrane different from the remaining units in the lower plate, or that they represent Hawasina continental slope units metamorphosed under high-*P*/*T* conditions (Oberhänsli *et al.*, 1999), are not supported by conclusive data.

2 The most likely protolith of the Ruwi tectonic mélange (Region I) is one of the members of the Late Cretaceous Muti Formation (Le Métour *et al.*, 1986; Robertson, 1987a, b; El-Shazly, 1994). The suggestion of Searle *et al.* (1994) that this mélange is part of the Haybi Complex is less likely. The Haybi Complex (a mixture of volcanics, olistostromes and exotic limestones) is always thrust on top of the unmetamorphosed Hawasina sediments (Searle *et al.*, 1980; Searle & Cooper, 1986), whereas the Ruwi mélange is sandwiched between the shelf units and the overthrust Hawasina cherts and serpentinites (Le Métour *et al.*, 1986; El-Shazly, 1994).

3 The bulk of the igneous crustal rocks of the Semail ophiolite crystallized between 97 and 94 Ma, as indicated by U–Pb zircon ages on plagiogranites (Tilton *et al.*, 1981), $^{40}Ar/^{39}Ar$ hornblende ages on plagiogranites, gabbros and veins (Hacker *et al.*, 1997), and radiolarian and foraminiferal ages on sediments on top of the volcanic sequences (Tippit *et al.*, 1981).

4 Amphibolites and greenschists, which constitute a metamorphic sole welded to the base of the Semail ophiolite, formed between 96 and 89 Ma, as indicated by $^{40}Ar/^{39}Ar$ and K–Ar data on hornblende, muscovite and biotite from these rocks (Lanphere, 1981; Hacker *et al.*, 1997). These data also show that the amphibolites cooled through 550 °C between 95 and 93 Ma, indicating rapid cooling that is characteristic of normal oceanic crust (Hacker, 1994; Hacker *et al.*, 1997).

5 Final emplacement of the Semail ophiolite onto the Oman continental margin took place between the end of the Santonian and the early Maastrichtian (84 & 74.5 Ma), as indicated by the Turonian to Santonian age of the Muti Formation (Le Métour *et al.*, 1986) which structurally underlies the ophiolite, and by the Maastrichtian age of the laterites and conglomerates unconformably overlying it (Coleman, 1981; Hopson *et al.*, 1981).

6 High-*P*/*T* metamorphism of the upper plate (Regions I & II) of Saih Hatat took place in the Late Cretaceous, probably between 80 and 70 Ma. This is supported by $^{40}Ar/^{39}Ar$ ages for metasedimentary rocks from the Ruwi mélange (El-Shazly & Lanphere, 1992) and white micas from calcschists in Region II (Miller *et al.*, 1998a). Although the interpretation of $^{40}Ar/^{39}Ar$ ages is fraught with uncertainties associated with applying this technique to high-*P*/*T* rocks (as pointed out earlier), these ages are considered reasonable because: (i) they are consistent with the Turonian to Santonian age assigned to the Muti Formation, the youngest unit in the upper plate metamorphosed under high-*P*/*T* conditions; (ii) the ages overlap with the timing of ophiolite emplacement, a likely cause of high-

P/*T* metamorphism (e.g. Goffé *et al.*, 1988; El-Shazly, 1994, 1995); and (iii) the ages are consistent with the stratigraphic ages of the oldest unmetamorphosed sedimentary rocks that overlie the ophiolitic sequence unconformably (e.g. Coleman, 1981). The apparent success of $^{40}Ar/^{39}Ar$ dating of the high-*P*/*T* metamorphism of the upper plate rocks as opposed to its failure with the lower plate eclogites can be explained by the considerably lower pressure of metamorphism of the former (3–6.5 kbar for Region I and 6.5–9 kbar for Region II; see below), and the apparent tendency of white mica to incorporate excess Ar at higher pressures (e.g. Sherlock *et al.*, 1999). Following this line of reasoning, a K–Ar age of 95 ± 4 Ma on white mica from a calcschist from the deeper units of Region II (Montigny *et al.*, 1988) is considered unlikely to be geologically meaningful and is attributed to excess Ar.

7 Eclogite facies metamorphism in the lower plate of Saih Hatat (Region III) took place shortly before 78 ± 2 Ma, the time at which phengite cooled through its blocking temperature for Sr (500 °C). This interpretation is compatible with the $^{40}Ar/^{39}Ar$ maximum ages obtained for phengite from all three metamorphic zones (El-Shazly & Lanphere, 1992; Miller *et al.*, 1999), and overlaps with the timing of high-*P*/*T* metamorphism in the upper plate.

8 The eclogite facies rocks cooled through 210 °C at *c.* 68 ± 2 Ma, and through the 100 °C isotherm at *c.* 54 ± 3 Ma, as indicated by fission track ages on zircon and apatite, respectively (Saddiqi *et al.*, 1995; Poupeau *et al.*, 1998). Apatite fission track ages on upper plate rocks (Region II) indicate that they cooled through the 100° C isotherm between 57 and 40 Ma (Poupeau *et al.*, 1998).

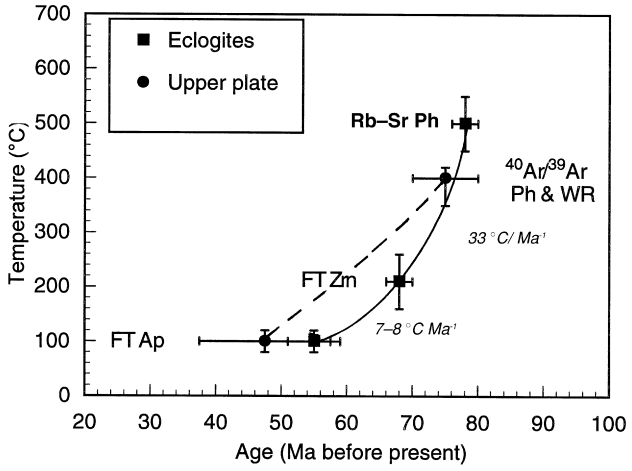

Fig. 7. Temperature–time curves for the lower plate eclogite facies rocks (filled squares) and the upper plate (Region II) schists (filled circles; broken curve), constrained by Rb–Sr (this study), fission track (FT) data (Saddiqi *et al.*, 1995; Poupeau *et al.*, 1998) and $^{40}Ar/^{39}Ar$ data (El-Shazly & Lanphere, 1992; Miller *et al.*, 1998a). Cooling rates for the lower plate rocks are given in italics. Cooling curves for both plates probably converge at the 100 °C isotherm at *c.* 55 Ma, after which both plates were exhumed at the same rate by erosion.

Petrological constraints

1 The amphibolites of the metamorphic sole formed at a temperature of 775–875 °C (Searle & Malpas, 1980; Ghent & Stout, 1981) and a minimum pressure of 8.5 kbar (based on the occurrence of kyanite in a garnet amphibolite; Gnos, 1998). Pressure estimates of 11–13 kbar (Gnos, 1998) are fraught with uncertainties as they are based on intersections of thermodynamically calculated stable and metastable equilibria in the system Na_2O–CaO–MgO–Al_2O_3–SiO_2–H_2O (NCMASH).

2 The Ruwi mélange of Region I, Saih Hatat, was metamorphosed at 280–320 °C and 3–6.5 kbar. Peak *P*–*T* conditions of metamorphism of the deepest units in the upper plate (Region II) are estimated at 380–430 °C and 6.5–9 kbar (El-Shazly, 1994, 1995, 1996). Higher pressure estimates, such as those of Vidal *et al.* (1992), are suspect (cf. El-Shazly, 1996). All of these units followed clockwise *P*–*T* paths (El-Shazly, 1994, 1995).

3 The lower plate rocks display an eastward increase in metamorphic grade from 400–460 °C, 6.5–8.5 kbar for zone A to 500–580 °C, 12–16 kbar for zone C. Higher pressure estimates for the As-Sifah eclogites (e.g. Searle *et al.*, 1994) based on empirical geobarometers are inconsistent with phase relations in interlayered cofacial metapelites and quartz–mica schists (El-Shazly *et al.*, 1997; El-Shazly, 2001). As long as mineral assemblages indicative of such high pressures have not been found in these rocks, we prefer to remain conservative in our pressure estimates, making use of reliable geobarometers and petrogenetic grid calculations.

4 All lower plate high-*P*/*T* metamorphic rocks followed clockwise *P*–*T* paths, with the eclogite facies rocks characterized by a segment of near-isothermal decompression between pressures of *c.* 12 kbar and *c.* 5 kbar at *c.* 500 °C, followed by another segment of near-isobaric cooling, as indicated by microthermometric measurements on solitary fluid inclusions in Cpx and quartz (El-Shazly & Sisson, 1999).

5 A pressure gap between the lower and upper plates exists and is most apparent in the eastern parts of Saih Hatat, where rocks metamorphosed at *c.* 6.5–9 kbar are juxtaposed against blueschist and eclogite facies rocks formed at 12–16 kbar. In western Saih Hatat, this gap is almost non-existent, where pressure estimates for metasediments and metabasites of the upper plate Hijam and Hatat Formations overlap with those of zone A in the lower plate. However, the Hatat and Hijam units are characterized by the occurrence of magnesioriebeckite/crossite and magnesiocarpholite, respectively, whereas zone A schists contain crossite and chloritoid but no Fe–Mg carpholite, which suggests higher temperature ($\pm P$) conditions for the

latter, and a possible pressure gap of < 1 kbar across the plate boundary in western Saih Hatat.

6 High-P/T metamorphism affected the basement, shelf and foreland basin units of Saih Hatat only. Rocks that structurally underlie the Semail ophiolite in other tectonic windows do not show evidence of high-P/T metamorphism.

Cooling rates

Combining the fission track ages of Saddiqi *et al.* (1995) and Poupeau *et al.* (1998) with our Rb–Sr ages for the eclogite facies rocks of As-Sifah leads us to suggest that these rocks may have had two stages of cooling. During the first stage, which occurred between 78 and 68 Ma, the eclogite facies rocks cooled at a rate of *c.* 33 °C Ma^{-1}. Between 68 and 54 Ma, the cooling rate decreased to 7–8 °C Ma^{-1} (Fig. 7). On the other hand, the cooling rate of the upper plate units is estimated at 7–11 °C Ma^{-1} based on the fission track ages of Poupeau *et al.* (1998) and the assumption that these rocks reached their peak temperature at *c.* 80 Ma.

Structural constraints

1 Lower plate units are deformed into a series of closed folds that verge to the north or north-east in zone A, and which become sheath folds verging ENE in zone C. These units are characterized by a penetrative foliation that has been folded and transposed in the highest grade rocks of zone C.

2 A NE-trending mineral lineation which post-dates the growth of most high-P/T porphyroblasts is well developed in the lower plate rocks. Michard *et al.* (1994) and Miller *et al.* (1999) associated this lineation with sheath folding and top-to-the-NE shear sense indicators, and interpreted it to have developed during extension.

3 S–C fabrics and extensional crenulation cleavages that developed in the lower plate rocks under greenschist facies conditions indicate a down-to-the-NE sense of shear (Michard *et al.*, 1994; Searle *et al.*, 1994; Miller *et al.*, 1998a).

4 In the northern parts of the upper plate (Region II), folds with S- or SW-directed vergence predominate. The penetrative foliation of these units is axial planar and nearly parallel to structural breaks within this plate (e.g. Michard *et al.*, 1994; Miller *et al.*, 1999).

5 A NE-trending mineral lineation in Region II (upper plate) is related to SW-directed compressional fabrics (Michard *et al.*, 1994). Miller *et al.* (1999) reported rare shear bands at the structurally deepest levels of this plate which indicate top-to-the-NE transport.

6 The low-angle ductile shear boundary between the lower and upper plates cross-cuts nappe structures in both plates indicating relatively late movement along this boundary (Gregory *et al.*, 1998).

7 The metamorphic sole rocks which structurally overlie the Saih Hatat high-P/T rocks are characterized by a foliation and bedding which are nearly parallel to their tectonic contact with the overlying Semail ophiolite (e.g. Ghent & Stout, 1981).

8 The base of the Semail ophiolite is characterized by mylonitized harzburgites with a foliation similar to that in the underlying amphibolites of the metamorphic sole (Boudier & Coleman, 1981). The ophiolite itself is locally folded, with the Semail 'thrust' and Moho overturned in places (Gregory *et al.*, 1998).

9 The Semail thrust has been reactivated as a low-angle normal fault (e.g. Michard *et al.*, 1994; Gregory *et al.*, 1998), probably during the Tertiary events that led to the formation of the Saih Hatat, Jebel Akhdar and Hawasina domal structures.

Proposed tectonic model for the evolution of Saih Hatat

In the Early Cretaceous at *c.* 96 Ma, crustal rocks of the Semail ophiolite crystallized at the site of a fast, mid-oceanic spreading centre located E and NE of the Oman continental margin (Boudier & Nicolas, 1985; Fig. 8a). Several authors have suggested that this spreading centre was located in a back-arc basin (e.g. Lippard *et al.*, 1986; Searle & Cox, 1999), but this is still debated (e.g. Coleman, 1981; Beurrier *et al.*, 1989). Between 96 and 95 Ma, a change in plate motion caused Africa to begin its counterclockwise rotation towards Eurasia, which in turn resulted in intraoceanic thrusting, marking the first stages of ophiolite obduction (Fig. 8b). Although this thrust was described by Searle *et al.* (1994) and Searle & Cox (1999) as a subduction zone, we prefer the term 'intraoceanic thrust' to describe its low-angle nature (15°), in line with the terminology and conclusions of Cloos (1993). The location of this detachment is controversial (cf. Hacker & Gnos, 1997; Searle & Cox, 1999), but it must have occurred close to (or at?) the site of the mid-oceanic ridge (Boudier *et al.*, 1988) in order to account for the high temperatures reached by the underplated crust as it was metamorphosed to amphibolites of the sole. This metamorphism occurred at a depth of *c.* 25 km to account for the P–T conditions estimated by Ghent & Stout (1981) and Gnos (1998). Fluids driven off from the underplated slab during upper amphibolite facies metamorphism infiltrated the mantle rocks of the overthrust plate, which may have triggered partial melting in the hanging wall. Melts produced by this process eventually penetrated the mantle and crustal sequence of the overthrust plate and the metamorphic sole, giving rise to the intrusive and extrusive rocks of the middle Cenomanian to late Turonian 'second magmatic event (M2)' of the Semail ophiolite (e.g. Le Métour *et al.*, 1995) and leucogranitic dykes (Cox *et al.*, 1999). Rocks formed during M2 are characterized by a weak geochemical arc signature (Beurrier *et al.*, 1989).

As the Semail ophiolite advanced towards the continental margin of Oman, the amphibolites, now welded to its base, were dragged with the ophiolite across the Hawasina basin. These amphibolites cooled

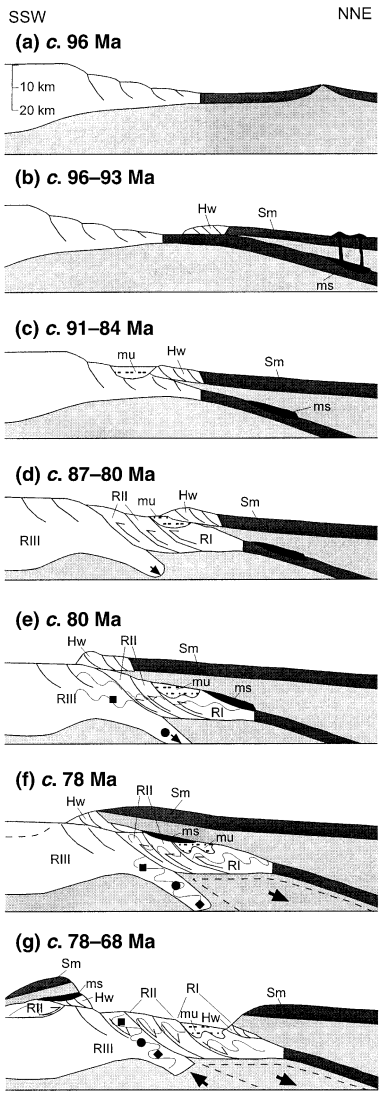

Fig. 8. Simplified cartoon showing the stages of evolution of the continental margin of Saih Hatat with special emphasis on the formation and denudation of the high-pressure metamorphic rocks. (a) *c.* 96 Ma (Cenomanian). Crystallization of the Semail oceanic crust. (b) 96–93 Ma (Cenomanian). Intraoceanic detachment, formation of the metamorphic sole and M2 magmatism. (c) 91–84 Ma (Turonian–Santonian). Deposition of the Muti Formation in a foreland basin. (d) 87–80 Ma (Santonian–Campanian). Intracontinental subduction and thickening of the Oman continental margin. (e) *c.* 80 Ma (Campanian). Emplacement of the Semail ophiolite, metamorphism of the upper plate and continued subduction of the lower plate. (f) *c.* 78 Ma (Campanian). Final emplacement of the ophiolite, choking of the subduction zone and incipient tectonic exhumation of lower plate aided by ductile thinning of mantle wedge. (g) 78–68 Ma (Campanian–Maastrichtian). Tectonic exhumation of high-*P*/*T* rocks and juxtaposition of upper plate rocks against lower plate ones. Exhumation of the high-*P*/*T* rocks during the Tertiary beyond stage (g) took place at a slower rate, primarily by erosion. Filled square, crossite–epidote schists of zone A; filled circle, zone B blueschists; filled diamond, zone C eclogites. Sm, Semail ophiolite; Hw, Hawasina sediments; ms, metamorphic sole; mu, Muti Formation; RII, Region II; RIII, Region III.

rapidly through 550 °C between 95 and 93 Ma (Hacker *et al.*, 1997) as they were thrust onto colder rocks, which were in turn metamorphosed at lower temperature conditions and welded to the base of the overriding slab to complete the formation of the metamorphic sole. As the ophiolite and metamorphic sole cooled and continued their advance towards the margin, continental slope sediments of the Hawasina basin were scraped off the overridden plate and bulldozed in front of the leading edge of the advancing ophiolite, hence largely escaping metamorphism (Fig. 8b).

As the ophiolite approached the continental margin of Oman, obduction continued because the continental crust was sufficiently thin along this margin (15 km for a 100 km thick lithosphere; Cloos, 1993). The impingement of the ophiolite onto the continental margin of Oman *c.* 91–84 Ma resulted in the formation of a foreland bulge and basin. The foreland basin migrated inboard with time as it filled with sediments of the Turonian–Santonian Muti Formation, locally derived from the continental margin by mass wasting of the foreland bulge (Robertson, 1987a) and from the Hawasina basin by the bulldozing effect of the advancing ophiolite. This produced a tectonic mélange in some parts of the Muti basin (Fig. 8c).

Between 87 and 80 Ma, when the continental margin of Saih Hatat was being tectonically loaded by the Semail ophiolite, intracontinental thrusting took place, possibly triggered by a sudden increase in the rate of plate convergence. This event led to the development of a NE-dipping subduction zone and two discrete plates structurally beneath the Semail ophiolite: an upper plate consisting of folded and imbricated basement, continental shelf and foreland basin units (including the newly formed Muti tectonic mélange), and a more coherent lower plate (Region III), both anchored to their lithospheric mantle (Fig. 8d). Subduction of the lower plate to depths > 15 km resulted in the formation of blueschists and eclogites within its crust, which eventually became separated from the upper plate by a lithospheric mantle wedge thickening to the NE (Fig. 8d). In the meantime, the emplacement of the ophiolite onto the continental margin caused high-*P*/*T* metamorphism of the upper plate units, and their simultaneous folding (with S- to SW-directed vergence) and thrusting (Fig. 8e).

Between 80 and 78 Ma, when the leading edge of the lower plate reached a depth of 40–50 km, the continental margin, with its thin crust (15 km), was either consumed by subduction (lower plate) or overridden by the ophiolite (upper plate). As convergence continued, and thicker continental crust (*c.* 30 km) attempted to enter the subduction zone, it instead choked it due to its positive buoyancy (Cloos, 1993). This in turn initiated the exhumation of the lower plate rocks, most likely along the trace of the subduction thrust as it was reactivated as a normal fault at *c.* 78 Ma. As convergence and emplacement of the ophiolite continued simultaneously with the tectonic

exhumation of the lower plate rocks, the lithospheric mantle wedge separating the two plates (Regions II and III) underwent ductile thinning (Fig. 8f). Tectonic exhumation and ductile thinning of this wedge both led to the development of the NE-vergent nappes (which telescoped the three metamorphic zones of the lower plate), the NE-trending lineation and other extensional structures in the lower plate (e.g. Michard *et al*., 1994). Eventually, these two processes led to the juxtaposition of the upper plate rocks onto the lower plate ones (Fig. 8g).

By the end of the Campanian (*c*. 75 Ma), compression at the Oman margin waned, possibly as a result of the initiation of subduction of Tethyan oceanic lithosphere along a N- to NE-dipping zone beneath the Iran continental margin. With this new plate configuration, buoyancy forces continued to drive the lower plate rocks towards the surface, initiating the updoming of the Saih Hatat area. Normal faulting within the upper plate and the overlying Semail ophiolite (which broke into discrete blocks flanking Saih Hatat, Fig. 8g) was the main mechanism for the exhumation of high-*P*/*T* rocks at this stage. In the Maastrichtian, the Semail ophiolite was exposed to subaerial weathering and erosion for a short period of time, marked by the formation of laterites that overlie it unconformably (Coleman, 1981). By the end of the Maastrichtian (*c*. 68 Ma), the ophiolite had slid off the Saih Hatat protodome to the north and south, whereas the lower plate eclogites had been exhumed to a depth of *c*. 14 km as indicated by the fission track data of Saddiqi *et al*. (1995) on zircon (assuming that the geothermal gradients had relaxed from *c*. 10–12 °C km^{-1}, attained during high-*P*/*T* metamorphism, to *c*. 15 °C km^{-1}).

During the late Palaeocene to early Eocene, a rise in sea level caused the deposition of conglomerates, marls and limestones on top of the Semail ophiolite in basins to the north, east and south-west of Saih Hatat, which remained a tectonic high undergoing erosion (Le Métour *et al*., 1995). At the same time, the high-*P*/*T* metamorphic rocks continued their journey to the surface, although at a much lower rate (*c*. 0.4–0.8 mm yr^{-1}; assuming that the geothermal gradient continued to relax to *c*. 20 °C km^{-1}). This process was driven primarily by erosion and mass wasting (processes compatible with these rates, e.g. Burbank & Beck, 1991; Burbank *et al*., 1996; Blythe, 1998), but may have also been aided by normal faulting in the upper plate. In the Eocene, subduction beneath the Makran continental margin of Iran had become well developed, causing the fully fledged development of the domal structures of Saih Hatat, Jebel Akhdar and Hawasina windows. By 55 Ma, the eclogites had been exhumed to the same level as some units in Region II (Poupeau *et al*., 1998). Between 53 and 19 Ma, the high-*P*/*T* rocks of both plates continued to be exhumed by erosion. A Miocene–Pliocene compressional event culminating at *c*. 7–4 Ma caused minor heating of these rocks as indicated by fission track length data on apatite (Poupeau *et al*., 1998). Erosion, normal faulting and mass wasting resumed in Saih Hatat until the eclogite facies rocks were finally exposed on the surface.

Our proposed tectonic model is based on ideas presented in other models for the formation and exhumation of high-*P*/*T* rocks (e.g. Philippot, 1990), and is very similar to that of Michard *et al*. (1994). Although this model accounts for the geochronological and petrological data available, and explains the pressure gaps between the upper and lower plates and the differences in directions of fold vergence in both plates, it is still an oversimplified two-dimensional speculative model. Models involving oblique subduction (Avé Lallement & Guth, 1990) and subsequent extrusion should be entertained, particularly in the light of recent work suggesting late Maastrichtian to early Tertiary compression along the SE margin of Oman culminating in the emplacement of the Masirah island ophiolite (e.g. Immenhauser *et al*., 2000). More research is therefore needed to: (i) identify the causes of intracontinental subduction; (ii) provide structural evidence for the proposed mechanisms of exhumation of the high-*P*/*T* rocks; (iii) quantify the forces necessary to initiate exhumation; (iv) explain the development of a static greenschist facies overprint on the crossite–epidote schists of zone A (El-Shazly & Lanphere, 1992), when such an overprint is associated with extensional fabrics in zones B and C; and (v) account for the restriction of Fe–Mg carpholite grade high-*P*/*T* metamorphism to the Saih Hatat area, when it is attributed to the tectonic loading of the continental margin by the ophiolite.

ACKNOWLEDGEMENTS

This study was supported by funds from the Deutsche Forschungsgemeinschaft to Bröcker, and grants ES/97/03 from the College of Science, Sultan Qaboos University to El-Shazly and NSF EAR-9725667 to Hacker. Thorough reviews by Professor J. Selverstone and Drs V. B. Sisson and M. Sullivan have improved the manuscript substantially. El-Shazly and Hacker are both grateful to the Ministry of Commerce and Industry, particularly Mr. M. Kassim and Dr H. Al-Azry, for facilitating field work in Oman. Dr J. Rogers is thanked for drafting fig. 1, and T. Crane for help with fig. 8.

REFERENCES

Arnaud, N. O. & Kelley, S. P., 1995. Evidence for excess argon during high pressure metamorphism in the Dora Maira Massif (western Alps, Italy), using an ultraviolet laser ablation microprobe $^{40}Ar/^{39}Ar$ technique. *Contributions to Mineralogy and Petrology*, **121,** 1–11.

Avé Lallement, H. & Guth, L. R., 1990. Role of extensional tectonics in exhumation of eclogites and blueschists in an oblique subduction setting: Northeastern Venezuela. *Geology*, **18,** 950–953.

Beurrier, M., Ohnenstetter, M., Cabanis, B., Lescuyer, J.L., Tegyey, M. & Le Métour, J., 1989. Geochemie des filons

doleritiques et des roches volcaniques ophiolitiques de la nappe de Semail: contraintes sur leur origine geotectonique au Cretace superieur. *Bulletin Géologique de France*, **2 (8),** 205–219.

Blanckenburg, F. V., Villa, I. M., Baur, H., Morteani, G. & Steiger, R. H., 1989. Time calibration of a PT-path from the Western Tauern Window, Eastern Alps: the problem of closure temperatures. *Contributions to Mineralogy and Petrology*, **101,** 1–11.

Blythe, A. E., 1998. Active tectonics and ultrahigh-pressure rocks. In: *When Continents Collide: Geodynamics and Geochemistry of Ultrahigh-Pressure Rocks* (eds Hacker, B. R. & Liou, J. G), pp. 141–160. Kluwer Academic Publishers, Dordrecht.

Boudier, F. & Coleman, R. G., 1981. Cross section through the peridotite in the Semail ophiolite, southeastern Oman. *Journal of Geophysical Research*, **86,** 2573–2592.

Boudier, F. & Nicolas, A., 1985. Harzburgites and lherzolites in subtypes in ophiolitic and oceanic environments. *Earth and Planetary Science Letters*, **76,** 84–92.

Boudier, F., Ceulleneer, G. & Nicolas, A., 1988. Shear zones, thrusts and related magmatism in the Oman ophiolite: initiation of thrusting on an oceanic ridge. *Tectonophysics*, **51,** 275–296.

Bröcker, M. & Franz, L., 1998. Rb–Sr isotope studies on Tinos Island (Cyclades, Greece): additional time constraints for metamorphism, extent of infiltration controlled overprinting and deformational activity. *Geological Magazine*, **135,** 369–382.

Burbank, D. & Beck, R., 1991. Rapid long-term rates of denudation. *Geology*, **19,** 1169–1172.

Burbank, D., Leland, J., Fielding, E., et al., 1996. Bedrock incision, rock uplift and threshold hillslopes in the northwestern Himalayas. *Nature*, **379,** 505–510.

Chemenda, A. I., Mattauer, M. & Bokun, A. N., 1996. Continental subduction and a mechanism for exhumation of high pressure metamorphic rocks: new modelling and field data from Oman. *Earth and Planetary Science Letters*, **143,** 173–182.

Cloos, M., 1993. Lithospheric buoyancy and collisional orogenesis: subduction of oceanic plateaus, continental margins, island arcs, spreading ridges, and seamounts. *Geological Society of America, Bulletin*, **105,** 715–737.

Coleman, R. G., 1981. Tectonic setting for ophiolite obduction in Oman. *Journal of Geophysical Research*, **86,** 2497–2508.

Cox, J., Searle, M. P. & Pedersen, R., 1999. The petrogenesis of leucogranitic dykes intruding the northern Semail ophiolite, United Arab Emirates: field relationships, geochemistry and Sr/Nd isotope systematics. *Contributions to Mineralogy and Petrology*, **137,** 267–287.

Cumbest, R. J., Johnson, E. L. & Onstott, T. C., 1994. Argon composition of metamorphic fluids: implications for $^{40}Ar/^{39}Ar$ geochronology. *Geological Society of America, Bulletin*, **106,** 942–951.

Dallmeyer, R. D., Peucat, J. J., Hirajima, T. & Ohta, Y., 1990. Tectonothermal chronology within a blueschist–eclogite complex, west-central Spitsbergen, Svalbard: evidence from $^{40}Ar/^{39}Ar$ and Rb–Sr mineral ages. *Lithos*, **24,** 291–304.

Dalrymple, G. B. & Lanphere, M. A., 1974. $^{40}Ar/^{39}Ar$ age spectra of some undisturbed terrestrial samples. *Geochimica et Cosmochimica Acta*, **38,** 359–372.

El-Shazly, A. K., 1994. Petrology of lawsonite, pumpellyite and sodic amphibole-bearing rocks from Saih Hatat, NE Oman. *Journal of Metamorphic Geology*, **12,** 23–48.

El-Shazly, A. K., 1995. Petrology of Fe–Mg carpholite-bearing metasediments from NE Oman. *Journal of Metamorphic Geology*, **13,** 379–396.

El-Shazly, A. K., 1996. Petrology of Fe–Mg carpholite-bearing metasediments from NE Oman: reply to comments by Vidal and Theye. *Journal of Metamorphic Geology*, **14,** 386–397.

El-Shazly, A. K., 2000. Are pressures in blueschists and eclogites overestimated? The case from Oman. *Lithos*, in press.

El-Shazly, A. K. & Coleman, R. G., 1990. Metamorphism in the Oman Mountains in relation to the ophiolite emplacement. In: *The Geology and Tectonics of the Oman Region. Geological Society, London, Special Publication*, 49 (eds Robertson, A. H. F., Searle, M. P. & Ries, A.), pp. 475–495. Geological Society, London.

El-Shazly, A. K. & Lanphere, M. A., 1992. Two high pressure metamorphic events in NE Oman: evidence from $^{40}Ar/^{39}Ar$ dating and petrological data. *Journal of Geology*, **100,** 731–751.

El-Shazly, A. K. & Liou, J. G., 1991. Glaucophane chloritoid bearing assemblages from NE Oman: petrologic significance and a petrogenetic grid for high P/T metapelites. *Contributions to Mineralogy and Petrology*, **107,** 180–201.

El-Shazly, A. K. & Sisson, V. B., 1999. Retrograde evolution of eclogites and blueschists from NE Oman: evidence from fluid inclusions and petrological data. *Chemical Geology*, **154,** 193–223.

El-Shazly, A. K., Coleman, R. G. & Liou, J. G., 1990. Eclogites and blueschists from NE Oman: petrology and P–T evolution. *Journal of Petrology*, **31,** 629–666.

El-Shazly, A. K., Worthing, M. A., Jayawardane, J. & Varne, R., 1994. Geochemistry of metamorphosed mafic rocks from Saih Hatat: insights into the pre-obduction history of NE Oman. *Journal of the Geological Society of London*, **151,** 999–1016.

El-Shazly, A. K., Worthing, M. A. & Liou, J. G., 1997. Interlayered eclogites, blueschists and epidote amphibolites from NE Oman: a record of protolith compositional control and limited fluid infiltration. *Journal of Petrology*, **38,** 1461–1487.

Gebauer, D., Schertl, H.-P., Brix, M. & Schreyer, W., 1997. 35 Ma old ultrahigh-pressure metamorphism and evidence for very rapid exhumation in the Dora Maira Massif, Western Alps. *Lithos*, **41,** 5–24.

Ghent, E. D. & Stout, M. Z., 1981. Metamorphism at the base of the Semail ophiolite, Oman. *Journal of Geophysical Research*, **86,** 2557–2571.

Glennie, K. W., Boeuf, M. G. A., Hughes Clark, M. H. W., Moody-Stuart, M., Pilaar, W. F. & Reinhardt, B. M., 1974. Geology of the Oman mountains. *Verhandelingen van het Koninklijk Nederlands Geologischs Mijnbouwkundig Genootschap*, **31,** 1–423.

Goffé, B., Michard, A., Kienast, J. R. & Le Mer, O., 1988. A case of obduction related high P low T metamorphism in upper crustal nappes, Arabian continental margin, Oman: P–T paths and kinematic interpretation. *Tectonophysics*, **151,** 363–386.

Gnos, E., 1998. Peak metamorphic conditions of garnet amphibolites beneath the Semail ophiolite: implications for an inverted pressure gradient. *International Geology Review*, **40,** 281–304.

Gregory, R. T., Gray, D. R. & Miller, J. McL., 1998. Tectonics of the Arabian margin associated with the formation and exhumation of high pressure rocks, Sultanate of Oman. *Tectonics*, **17,** 657–670.

Hacker, B. R., 1994. Rapid emplacement of young oceanic lithosphere. *Science*, **265,** 1563–1565.

Hacker, B. R. & Gnos, E., 1997. The conundrum of Semail: explaining the metamorphic history. *Tectonophysics*, **279,** 215–226.

Hacker, B. R. & Wang, Q. C., 1995. Ar/Ar geochronology of ultrahigh-pressure metamorphism in central China. *Tectonics*, **14,** 994–1006.

Hacker, B. R., Mosenfelder, J. L. & Gnos, E., 1997. Rapid ophiolite emplacement constrained by geochronology and thermal considerations. *Tectonics*, **15,** 1230–1247.

Hammerschmidt, K. & Franz, G., 1992. Retrograde evolution of eclogites: evidence from microstructures and $^{40}Ar/^{39}Ar$ white mica dates, Munchberg Massif, northern Bavaria. *Contributions to Mineralogy and Petrology*, **111,** 113–125.

Hannula, K. A. & McWilliams, M. O., 1995. Reconsideration of the age of blueschist facies metamorphism on the Seward Peninsula, Alaska, based on phengite $^{40}Ar/^{39}Ar$ results. *Journal of Metamorphic Geology*, **13,** 125–139.

Hopson, C. A., Coleman, R. G., Gregory, R. T., Pallister, J. S. & Bailey, E. H., 1981. Geologic section through the Muscat–Ibra transect, southeastern Oman Mountains. *Journal of Geophysical Research*, **86,** 2527–2544.

Hunziker, J. C., Desmons, J. & Martinotti, G., 1989. Alpine thermal evolution in the central and western Alps. In: *Alpine Tectonics. Geological Society, London, Special Publication*, 45 (eds Coward, M. P., Dietrich, D. & Park, R. G.), pp. 353–367. Geological Society, London.

Immenhauser, A., Schreurs, G., Gnos, E., Oterdoom, H. W. & Hartmann, B., 2000. Late Paleozoic to Neogene geodynamic evolution of the northeastern Oman margin. *Geological Magazine*, **137,** 1–18.

Inger, S., Ramsbotham, W., Cliff, R. A. & Rex, D. C., 1996. Metamorphic evolution of the Sesia-Lanzo Zone, Western Alps: time constraints from multi-system geochronology. *Contributions to Mineralogy and Petrology*, **126,** 152–168.

Kirschner, D. L., Cosca, M. A., Masson, H. & Hunziker, J. C., 1996. Staircase $^{40}Ar/^{39}Ar$ spectra of fine-grained white mica: timing and duration of deformation and empirical constraints on argon diffusion. *Geology*, **24,** 747–750.

Lanphere, M. A., 1981. K–Ar ages of metamorphic rocks at the base of the Semail ophiolite, Oman. *Journal of Geophysical Research*, **86,** 2777–2782.

Lanphere, M. A. & Dalrymple, G. B., 1976. Identification of excess ^{40}Ar by the $^{40}Ar/^{39}Ar$ age spectrum technique. *Earth and Planetary Science Letters*, **32,** 141–148.

Le Métour, J., de Gramont, X. & Villey, M., 1986. *Geological Map of Masqat and Quryat, Sheets NF40-4A, NF40-4D. Scale 1 : 100, 000.* Ministry of Petroleum and Minerals, Directorate General of Minerals, Sultanate of Oman.

Le Métour, J., Michel, J. C., Béchennec, F., Platel, J. P. & Roger, J., 1995. *Geology and Mineral Wealth of the Sultanate of Oman.* Ministry of Petroleum and Minerals Geological Documents, Sultanate of Oman.

Le Métour, J., Rabu, D., Tegyey, M., Bechennec, F., Beurrier, M. & Villey, M., 1990. Subduction and obduction: two stages in the Eo-Alpine tectonometamorphic evolution of the Oman Mountains. In: *The Geology and Tectonics of the Oman Region. Geological Society, London, Special Publication*, 49 (eds Robertson, A. H. F., Searle, M. P. & Ries, A. C.), pp. 327–339. Geological Society, London.

Li, S., Wang, S., Chen, Y., et al., 1994. Excess Ar in phengite from eclogite: evidence from dating of eclogite by Sm–Nd, Rb–Sr and $^{40}Ar/^{39}Ar$ methods. *Chemical Geology Isotope Geoscience*, **112,** 343–350.

Lippard, S. J., 1983. Cretaceous high pressure metamorphism in NE Oman and its relationship to subduction and ophiolite nappe emplacement. *Journal of the Geological Society, London*, **140,** 97–104.

Lippard, S. J., Shelton, A. W. & Gass, I. G., 1986. *The Ophiolite of Northern Oman.* Blackwell Scientific Publications, Oxford.

McDougall, I. & Harrison, T. M., 1988. *Geochronology and Thermochronology by the $^{40}Ar/^{39}Ar$ Method. Oxford Monographs, Geology and Geophysics*, 9. Oxford University Press, Oxford.

Michard, A., Bouchéz, J. L. & Ouazzani-Touhami, M., 1984. Obduction related planar and linear fabrics in Oman. *Journal of Structural Geology*, **6,** 39–49.

Michard, A., Goffé, B. & Ouazzani-Touhami, M., 1983. Obduction related high pressure, low temperature metamorphism in upper crustal materials, Muscat, Oman. *Terra Cognita*, **3,** IA22–23.

Michard, A., Goffé, B., Saddiqi, O., Oberhänsli, R. & Wendt, A. S., 1994. Late Cretaceous exhumation of the Oman blueschists and eclogites: a two-stage extensional mechanism. *Terra Nova*, **6,** 404–413.

Miller, J. M. L., Gray, D. R. & Gregory, R. T., 1999. Exhumation of high pressure rocks in northeastern Oman. *Geology*, **26,** 235–238.

Miller, J. M. L., Gregory, R. T. & Gray, D. R., 1999. Geological and geochronological constraints on the exhumation of a high-pressure metamorphic terrane, Oman. In: *Exhumation Processes: Normal Faulting, Ductile Flow and Erosion. Geological Society, London, Special Publication*, 154 (eds Ring, U., Brandon, M. T., Lister, G. S. & Willet, S. D.), pp. 241–260. Geological Society, London.

Montigny, R., Le Mér, O., Thuizat, R. & Whitechurch, H., 1988. K–Ar and $^{40}Ar/^{39}Ar$ study of metamorphic rocks associated with the Oman ophiolite: tectonic implications. *Tectonophysics*, **151,** 345–362.

Oberhänsli, R., Wendt, A. S., Goffé, B. & Michard, A., 1999. Detrital chromites in metasediments of the East Arabian continental margin in the Saih Hatat area: constraints for the paleogeographic setting of the Hawasina and Semail basins. *International Journal of Earth Sciences (Geologisches Raundschau)*, **88,** 13–25.

Philippot, P., 1990. Opposite vergence of nappes and crustal extension in the French–Italian western Alps. *Tectonics*, **9,** 1143–1164.

Poupeau, G., Saddiqi, O., Michard, A., Goffé, B. & Oberhänsli, R., 1998. Late thermal evolution of the Oman Mountains subophiolitic windows: apatite fission track thermochronology. *Geology*, **26,** 1139–1142.

Purdy, J. W. & Jäger, E., 1976. K–Ar ages on rock-forming minerals from the central Alps. *Memoria Instituto Geologica e Mineralogica, Universita di Padova*, **30**.

Reddy, S. M., Kelley, S. P. & Wheeler, J., 1996. A $^{40}Ar/^{39}Ar$ laser probe study of micas from the Sesia Zone, Italian Alps: implications for metamorphic and deformation histories. *Journal of Metamorphic Geology*, **14,** 493–508.

Robertson, A. H. F., 1987a. Upper Cretaceous Muti Formation: transition of a Mesozoic carbonate platform to a foreland basin in the Oman Mountains. *Sedimentology*, **34,** 1123–1142.

Robertson, A. H. F., 1987b. The transition from a passive margin to an Upper Cretaceous foreland basin related to ophiolite emplacement in the Oman Mountains. *Geological Society of America, Bulletin*, **99,** 633–653.

Ruffet, G., Féraud, G., Ballévre, M. & Kienast, J. R., 1995. Plateau ages and excess argon in phengites: an $^{40}Ar/^{39}Ar$ laser probe study of Alpine micas (Sesia Zone, Western Alps, northern Italy). *Chemical Geology*, **121,** 327–343.

Saddiqi, O., Poupeau, G., Michard, A., Goffé, B. & Oberhänsli, R., 1995. Exhumation des roches metamorphiques HP-LT d'Oman: Datation par traces de fission sur zircons. *Paris, Academie des Sciences, Comptes Rendus*, **320,** 1071–1077.

Scaillet, S., Féraud, G., Ballèvre, M. & Amouric, M., 1992. Mg/Fe and $[(Mg,Fe)Si\text{-}Al_2]$ control on Ar behaviour in high pressure white micas: a $^{40}Ar/^{39}Ar$ continuous laser probe study from the Dora Maira nappe of the internal western Alps, Italy. *Geochimica et Cosmochimica Acta*, **56,** 2851–2872.

Schermer, E. R., Lux, D. R. & Burchfiel, B. C., 1990. Temperature–time history of subducted continental crust, Mount Olympos Region, Greece. *Tectonics*, **9,** 1165–1195.

Searle, M. P. & Cooper, 1986. Structure of the Hawasina Window culmination, central Oman Mountains. *Transactions of the Royal Society of Edinburgh: Earth Sciences*, **77,** 143–156.

Searle, M. P. & Cox, J., 1999. Tectonic setting, origin, and obduction of the Oman ophiolite. *Geological Society of America, Bulletin*, **111,** 104–122.

Searle, M. P. & Malpas, J., 1980. Structure and metamorphism of rocks beneath the Semail ophiolite of Oman and their tectonic significance in ophiolite obduction. *Transactions of the Royal Society of Edinburgh: Earth Sciences*, **71,** 247–262.

Searle, M. P., Lippard, S. J., Smewing, J. D. & Rex, D. C., 1980. Volcanic rocks beneath the Semail ophiolite nappe in the northern Oman mountains and their significance in the Mesozoic evolution of Tethys. *Journal of the Geological Society, London*, **137,** 589–604.

Searle, M. P., Waters, D. J., Martin, H. N. & Rex, D. C., 1994. Structure and metamorphism of blueschist–eclogite facies rocks from the northeastern Oman Mountains. *Journal of the Geological Society, London*, **151,** 555–576.

Sherlock, S., Kelley, S., Inger, S., Harris, N. & Okay, A., 1999.

$^{40}Ar/^{39}Ar$ and Rb–Sr geochronology of high-pressure metamorphism and exhumation history of the Tavsanli Zone, NW Turkey. *Contributions to Mineralogy and Petrology*, **137,** 46–58.

Sisson, V. B. & Onstott, T. C., 1986. Dating blueschist metamorphism: a combined $^{40}Ar/^{39}Ar$ and electron microprobe approach. *Geochimica et Cosmochimica Acta*, **50,** 2111–2117.

Steiger, R. H. & Jäger, E., 1977. Subcommission on geochronology: convention on the use of decay constants in geo- and cosmochronology. *Earth and Planetary Science Letters*, **36,** 359–362.

Tilton, G. R., Hopson, C. A. & Wright, J. E., 1981. Uranium–lead isotopic ages of the Semail ophiolite, Oman, with applications to Tethyan Ocean Ridge Tectonics. *Journal of Geophysical Research*, **86,** 2756–2762.

Tilton, G. R., Schreyer, W. & Schertl, H.-P., 1991. Pb–Sr–Nd isotopic behaviour of deeply subducted crustal rocks from the Dora Maira massif, western Alps, Italy II: what is the age of ultrahigh pressure metamorphism? *Contributions to Mineralogy and Petrology*, **108,** 22–33.

Tippit, P. R., Pessagno, E. A. & Smewing, J. D., 1981. The biostratigraphy of sediments in the volcanic unit of the Semail ophiolite. *Journal of Geophysical Research*, **86,** 2756–2762.

Tonarini, S., Villa, I. M., Oberli, F., et al., 1993. Eocene age of eclogite metamorphism in Pakistan Himalaya: implications for India–Eurasia collision. *Terra Nova*, **5,** 13–20.

Vidal, O., Goffé, B. & Theye, T., 1992. Experimental study of the stability of sudoite and magnesiocarpholite and calculation of a new petrogenetic grid for the system $FeO–MgO–Al_2O_3–SiO_2–H_2O$. *Journal of Metamorphic Geology*, **10,** 603–614.

Wendt, A. S., D'Arco, P., Goffé, B. & Oberhänsli, R., 1993. Radial cracks around α-quartz inclusions in almandine: constraints on the metamorphic history of the Oman Mountains. *Earth and Planetary Science Letters*, **114,** 449–461.

Wijbrans, J. R. & McDougall, I., 1986. $^{40}Ar/^{39}Ar$ dating of white micas from an Alpine high pressure metamorphic belt on Naxos (Greece): the resetting of the argon isotopic system. *Contributions to Mineralogy and Petrology*, **93,** 187–194.

York, D., 1969. Least squares fitting of a straight line with correlated errors. *Earth and Planetary Science Letters*, **5,** 320–324.

Received 11 February 2000; revision accepted 20 September 2000